Title:

Intestinal fructose metabolism/GLP-1/β-cell axis counteracts hyperglycemia after short-term fructose ingestion

Authors:

Naoya Murao[1,2*], Yusuke Seino[1,2], Risa Morikawa[1], Shihomi Hidaka[1], Takuya Haraguchi[1,2], Eisuke Tomatsu[1], Mutsumi Habara[1], Tamio Ohno[3], Norihide Yokoi[4], Norio Harada[5], Yoshitaka Hayashi[6], Yuichiro Yamada[1,2], Atsushi Suzuki[1]

Affiliations:

[1] Department of Endocrinology, Diabetes and Metabolism, Fujita Health University, School of Medicine, Toyoake, Japan

[2] Yutaka Seino Distinguished Center for Diabetes Research, Kansai Electric Power Medical Research Institute, Kyoto, Japan

[3] Graduate School of Medicine Center for Research of Laboratory Animals and Medical Research Engineering Division for Research of Laboratory Animals, Graduate School of Medicine, Nagoya University, Nagoya, Japan

[4] Laboratory of Animal Breeding and Genetics, Graduate School of Agriculture, Kyoto University, Kyoto, Japan

[5] Department of Endocrinology and Metabolism, School of Medical Sciences, University of Fukui, Fukui, Japan

[6] Department of Endocrinology, Research Institute of Environmental Medicine, Nagoya University, Nagoya, Japan

Orcid ID：

Naoya Murao*	0000-0002-7424-4476
Yusuke Seino	0000-0002-9099-3493
Risa Morikawa	0009-0004-1918-2649
Takuya Haraguchi	0009-0004-5218-8479
Tamio Ohno	0009-0005-9248-2880
Norihide Yokoi	0000-0002-5596-9754
Norio Harada	0000-0001-8720-1013

Yoshitaka Hayashi 0000-0002-7557-4303
Yuichiro Yamada 0000-0003-1623-0815
Atsushi Suzuki 0000-0003-0807-199X

*Corresponding author: Naoya Murao, M.D., Ph.D.
Departments of Endocrinology, Diabetes and Metabolism, Fujita Health University, School of Medicine, 1-98 Dengakugakubo, Toyoake, Aichi 4701192 Japan
Phone: +81-562-93-2699
Fax: +81-562-95-1879
E-mail: naoya.murao@fujita-hu.ac.jp

Keywords: Fructose; GLP-1; GIP; Incretin; Insulin.

ABSTRACT

Objective

The endocrine mechanisms linking fructose ingestion to glycemia remain unclear. This study revisited the mechanisms of fructose-induced incretin and insulin secretion to contextualize their roles in glycemic regulation following short-term fructose administration.

Methods

Mice were administered 20% fructose water ad libitum for 24 h. Plasma insulin and GLP-1 levels were compared with those of the water-administered controls. The mouse models included lean mice (C57BL/6J and NSY.B6-*a*/*a*), obese diabetic mice (NSY.B6-A^y/*a*), proglucagon-deficient mice (*Gcg*$^{-/-}$), glucose-dependent insulinotropic polypeptide (GIP) receptor-deficient mice (*Gipr*$^{-/-}$), and ATP-sensitive potassium channel (K_{ATP} channel)-deficient mice (*Kcnj11*$^{-/-}$). The involvement of intracellular fructose metabolism in GLP-1 secretion was investigated using GLUTag cells (a mouse L-cell line) and freshly isolated intestinal crypts.

Results

Fructose ingestion increased insulin, GLP-1, and GIP levels in lean mice. This insulin response was maintained in *Gipr*$^{-/-}$ mice but was eliminated in *Gcg*$^{-/-}$ mice or upon administration of the GLP-1 receptor antagonist exendin [9-39], indicating the requirement of GLP-1. Notably, multiple mouse strains deficient in fructose-induced insulin responses exhibit hyperglycemia following fructose ingestion, suggesting that insulin responses are essential for suppressing glycemia. Characterization of *Kcnj11*$^{-/-}$ mice and GLUTag cells corroborated the hypothesis that intestinal fructose metabolism regulates GLP-1 secretion through the ATP/ADP ratio and K_{ATP} channels. Metabolic tracing of the isolated intestinal crypts further suggested that fructolysis activity is coupled to the ATP/ADP ratio in the L-cell-resident niche.

Conclusion

Fructose ingestion stimulates GLP-1 secretion through intestinal fructose metabolism, which is required for the potentiation of insulin secretion. This pathway constitutes a counter-regulatory response to fructose-induced hyperglycemia.

1. ABBREVIATIONS

iAUC, incremental area under the curve
GIIS, glucose-induced insulin secretion
GIP, glucose-dependent insulinotropic polypeptide
GLP-1, glucagon-like peptide 1
K_{ATP} channel, ATP-sensitive potassium channel
SSB, sugar-sweetened beverage
VDCC, voltage-dependent Ca^{2+} channel

2. INTRODUCTION

Glucose and fructose are the two most abundant monosaccharides in the diet (Larke et al., 2023). Glucose enters enterocytes mainly through sodium-glucose cotransporter 1 (SGLT1) and partly through glucose transporter 2 (GLUT2) on the apical membrane. Fructose is transported into the enterocytes through glucose transporter 5 (GLUT5). Subsequently, both glucose and fructose are transported out of the enterocytes into the systemic circulation through GLUT2 on the basolateral membrane, with part of the fructose being converted to glucose within the enterocytes (Pepin et al., 2019).

Blood glucose levels are tightly maintained within the normal physiological range owing to glucose-induced insulin secretion (GIIS) from pancreatic β-cells. GIIS is regulated by multiple mechanisms. Primarily, pancreatic β-cells directly sense blood glucose and secrete insulin through a series of events: glucose metabolism leading to an increase in the intracellular ATP/ADP ratio, closure of ATP-sensitive potassium channels (K_{ATP} channels), depolarization of the cell membrane, opening of voltage-dependent calcium channels, and the influx of Ca^{2+} that stimulates the exocytosis of insulin-containing granules (Henquin, 2000; Henuin, 2009).

Additionally, gastrointestinal factors, most notably glucagon-like peptide 1 (GLP-1) and glucose-dependent insulinotropic polypeptide (GIP), further potentiate glucose-induced insulin secretion (GIIS). Following glucose ingestion, these incretins are secreted from L- and K-cells in the gut and activate their corresponding receptors in pancreatic β-cells (Seino et al., 2016; Santos-Hernández et al., 2024; Holst and Gromada, 2004). Mice lacking both incretin receptors have shown significant impairments in plasma insulin response and glucose tolerance following oral glucose administration (Hansotia et al., 2014; Preitner et al., 2004;

Ahrén et al., 2021). These findings underscore the critical role of incretins in the physiological plasma insulin response and glucose homeostasis (Nauck et al., 1986; Nauck and Meier, 2016).

However, it remains uncertain whether analogous mechanisms operate for fructose. Studies have demonstrated that fructose administration elevates plasma insulin and GLP-1 levels in rodents (Kuhre et al., 2014; Seino et al., 2015) and healthy humans (Kong et al., 1999; Kuhre et al., 2014). Although these effects were observed following acute intake of large doses of fructose (2–6 g/kg body weight), the relevance of these findings to physiological fructose consumption remains to be elucidated. Additionally, there is a lack of clear understanding of how these hormonal responses affect glucose homeostasis. To address these questions, we investigated metabolic responses following short-term (24h) ad libitum fructose ingestion across various mouse strains. We identified that the pathway consisting of intestinal fructose metabolism/GLP-1/β-cell serves as a crucial counterregulatory mechanism for fructose-induced hyperglycemia.

3. MATERIALS AND METHODS

3.1. Mice

NSY.B6-*Tyr*+ A^y/Hos mice, recently established by Ohno et al. (Ohno et al., 2022) were obtained from Hoshino Laboratory Animals (Ibaraki, Japan) and used for experiments at 19–20 weeks of age. C57BL/6JJcl (RRID:IMSR_JCL:JCL:MIN-0003) was purchased from CLEA Japan (Tokyo, Japan) and employed for experiments at 13 weeks of age.

Colonies of $Gcg^{gfp/+}$ and $Gcg^{gfp/gfp}$ (hereafter referred to as $Gcg^{-/-}$) mice (Hayashi et al., 2009), $Gipr^{-/-}$ mice (Miyawaki et al., 1999), and $Kcnj11^{-/-}$ mice (Miki et al., 1998) were maintained by intercrossing heterozygotes and homozygotes at Fujita Health University. All mice were housed under specific-pathogen-free conditions at 23 ± 2 °C and 55 ± 10% relative humidity with 12-hour light-dark cycles (8am–8pm), with ad libitum access to water and standard chow CE-2 (CLEA Japan, Tokyo, Japan). The health status of the mice was monitored regularly. All experiments were conducted using male mice. Body weight and blood glucose levels were measured at 9 am under ad libitum-fed conditions. All in vivo experiments were performed with the approval of APU22080 by the Institutional Animal Care and Use Committee of Fujita Health University, in compliance with the Guidelines for Animal Experimentation at Fujita Health University and current Japanese legislation

(Kagiyama et al., 2006). Efforts were made to minimize stress and pain during the experiments.

3.2. Fructose administration

The schedule of fructose administration is shown in Figure 1A. Mice were provided ad libitum access to 20% fructose as their sole water source for 24 h from 12:00 to 12:00. The control groups received water. From 8am to 12am on the second day, the mice were deprived of chow, while access to 20% fructose or water was maintained. The mice were subjected to fasting conditions with continuous access to fructose. Blood sampling and metabolic tests were conducted immediately after the administration period. For diazoxide treatment, diazoxide (Tokyo Chemical Industry, Tokyo, Japan, Cat# D5402) was pre-dissolved in dimethyl sulfoxide (DMSO) (FUJIFILM Wako Pure Chemical, Osaka, Japan, Cat# 041-29351) at a concentration of 1M and suspended in water or fructose solution at a final concentration of 10 mM, which was administered as previously described. For exendin [9-39] treatment, exendin [9-39] (Peptide Institute, Osaka, Japan, CAS: 133514-43-9, Cat# 4526-v) was dissolved in saline at 10 nmol/mL and injected intraperitoneally at a dose of 100 nmol/kg body weight immediately following a 24-hour fructose administration.

3.3. Measurement of plasma hormones

For hormone measurements, blood was collected from the tail vein of unanesthetized mice using heparinized capillaries. The blood was supplemented with 4% BD-P800 (Becton, Dickinson and Company, Franklin Lakes, NJ, USA, Cat# 366421) and centrifuged at 2000 × g, 4 °C for 20 min to obtain plasma. Insulin, GLP-1, GIP, and glucagon levels were measured using Ultra-sensitive Mouse Insulin ELISA (Morinaga Bioscience, Yokohama, Japan, Cat# M1104), Multi Species GLP-1 Total ELISA (Merck Millipore, Burlington, MA, USA, Cat# EZGLP1T-36K), Rat/Mouse GIP (total) ELISA (Merck Millipore, Burlington, MA, USA, Cat# EZRMGIP-55K), and Glucagon ELISA Kit (Mercodia, Uppsala, Sweden, Cat# 10-1281-01), respectively, in accordance with the manufacturer's instructions.

3.4. Measurement of plasma fructose

To assess plasma fructose levels after 24-hour ingestion, blood was collected from the tail vein of unanesthetized mice, as described in Section 2.1. Alternatively, portal blood was collected immediately after the mice were euthanized by isoflurane exposure. To test acute

fructose administration (Supplementary Figure 2, A–B), mice were fasted for 4 h with access to normal water. Aqueous fructose (2 g/10 mL) was administered via gavage at a dose of 2 g/kg body weight, and blood samples were obtained from the tail vein over 120 min. Blood was supplemented with 2 mM ethylenediaminetetraacetic acid (EDTA) and centrifuged at 2000 × g at 4 °C for 20 min to obtain plasma. For deproteinization, 37 μL of plasma was diluted with 370 μL of acetonitrile, vortexed, and centrifuged at 15000 × g at 4 °C for 10 min. The supernatant was vacuum-dried and stored at -20 °C until analysis. Fructose was quantified using an LCMS-8060 Triple Quadrupole Liquid Chromatograph Mass Spectrometer (Shimadzu, Kyoto, Japan, RRID:SCR_020515). The sample diluent was formulated by mixing 10 mM aqueous ammonium acetate and acetonitrile at a ratio of 15:85. Samples were reconstituted with 20 μL sample diluent and spiked with 100 μM $^{13}C_6$-fructose (Cambridge Isotope Laboratories, Tewksbury, MA, USA, CAS: 287100-63-4, Cat# CLM-1553-1) as an internal standard. Separations were performed using a reverse-phase column Unison UK-Amino, 150 × 2 mm silica-gel column (Imtakt, Kyoto, Japan, Cat# UKA25) at 55 °C with the gradient method with water and acetonitrile as the mobile phase at a flow rate of 0.4 mL/min. Mass spectrometry was performed in the multiple reaction monitoring (MRM) negative mode for fructose (m/z 179.0 > 89.0) and $^{13}C_6$-fructose (m/z 185.0 > 95.0).

3.5. Glucose and insulin tolerance tests

Glucose and insulin tolerance tests were performed as previously described (Murao et al. 2022). Following a 4-hour fast, aqueous glucose (1.5 g/10 mL) was administered via gavage at a dose of 1.5 g/kg body weight. Alternatively, human insulin (Humulin R, Eli Lilly, Indianapolis, IN, USA) was diluted with saline and administered intraperitoneally at a dose of 0.75 unit/kg body weight. Blood samples were collected from the tail vein over a 120-min period, during which mice were not allowed access to food and water. Blood glucose levels were measured using an Antsense Duo glucose analyzer (Horiba, Kyoto, Japan, Cat# LP-150).

3.6. Cell lines

MIN6-K8 cells were obtained from Professor Junichi Miyazaki (Osaka University) from cryopreserved original clones (Iwasaki et al., 2010). MIN6-K8 cells were cultured in Dulbecco's modified Eagle's medium (DMEM) containing 4500 mg/L glucose (Sigma-Aldrich, St. Louis, MO, USA, Cat# D5796) supplemented with 10% fetal bovine serum

(FBS) (BioWest, Nuaillé, France, Cat# S1400-500) and 5 ppm 2-mercaptoethanol. GLUTag cells (Drucker et al., 1994) were acquired from Dr. Akira Hirasawa (Kyoto University) with the permission of Professor Daniel Drucker. GLUTag cells were cultured in Dulbecco's modified Eagle's medium (DMEM) containing 1000 mg/L glucose (Sigma-Aldrich, St. Louis, MO, USA, Cat# D6046) supplemented with 10% FBS (BioWest, Nuaillé, France, Cat# S1400-500). All cells were maintained in a humidified incubator at 37 °C with 5% CO2.

3.7. Plasmids

GW1-PercevalHR was a generous gift from Professor Gary Yellen (Addgene plasmid # 49082; http://n2t.net/addgene:49082; RRID: Addgene_49082) (Tantama et al., 2013).

3.8. Reagents for in vitro experiments

For all in vitro experiments, Krebs-Ringer bicarbonate buffer-HEPES (KRBH: 133.4 mM NaCl, 4.7 mM KCl, 1.2 mM KH2PO4, 1.2 mM MgSO4, 2.5 mM CaCl2, 5 mM NaHCO3, 10 mM HEPES) supplemented with 0.1% bovine-serum albumin (Sigma-Aldrich, St. Louis, MO, USA, Cat# A6003) adjusted to pH 7.4 was used. Glucose was not added to KRBH unless otherwise specified. D-Fructose (FUJIFILM Wako Pure Chemical, Osaka, Japan, CAS: 57-48-7, Cat# 127-02765), Human GLP-1 7-36 amide (Peptide Institute, Osaka, Japan, CAS: 107444-51-9, Cat# 4344-v), and Human GIP (Peptide Institute, Osaka, Japan, CAS: 100040-31-1, Cat# 4178-s) were added to the KRBH only during the stimulation period. Nifedipine (FUJIFILM Wako Pure Chemical, Osaka, Japan, Cat# 14505781) and TEPP-46 (Selleck Chemicals, Houston, TX, USA, CAS: 1221186-53-3, Cat# S7302) were added during the pre-incubation and stimulation periods. GLP-1 and GIP were stored as a 100 μM solution in 0.1% aqueous acetic acid. Small-molecule reagents were stored as 1000× concentrate in dimethyl sulfoxide (DMSO) (FUJIFILM Wako Pure Chemical, Osaka, Japan, Cat# 041-29351). The reagents were diluted with KRBH immediately before the experiment. An equivalent volume of DMSO was added to the control when appropriate.

3.9. Isolation of pancreatic islets from mice

Digesting solution was formulated by supplementing 0.1w/v% Collagenase from Clostridium histolyticum (Sigma-Aldrich, St. Louis, MO, USA, Cat# C6885) to Hanks' balanced salt solution (136.9 mM NaCl, 5.4 mM KCl, 0.8 mM $MgSO_4$, 0.3 mM Na_2HPO_4, 0.4 mM KH_2PO_4, 4.2 mM $NaHCO_3$, 10 mM HEPES, 1.3 mM $CaCl_2$, 2 mM glucose). The

mice were euthanized by isoflurane exposure. Pancreas was digested by 10-min incubation at 37 °C following intraductal injection of digesting solution. Islets were hand-picked and separated from exocrine tissues, transferred to 60-mm non-treated plates (AGC Techno Glass, Shizuoka, Japan, Cat# 1010-060), and cultured overnight in RPMI-1640 (Sigma-Aldrich, St. Louis, MO, USA, Cat# R8758) supplemented with 10% FBS (BioWest, Nuaillé, France, Cat# S1400-500) and 1% penicillin-streptomycin solution (FUJIFILM Wako Pure Chemical, Osaka, Japan, Cat# 168-23191) at 37 °C with 5% CO_2 before the experiments.

3.10. Insulin secretion from islets

Insulin secretion from isolated islets was measured using the static incubation method, as previously described (Murao et al., 2022; Murao et al., 2025). Specifically, five size-matched islets were placed in each well of a 96-well plate (Corning, Glendale, AZ, USA, Cat# 353072) and were pre-incubated with 50 μL/well of KRBH supplemented with 2.8 mM glucose. Subsequently, 50 μL of KRBH supplemented with 19.4 mM glucose and 2 nM GLP-1 or GIP were added to the reaction, and the islets were incubated for an additional 30 min. The supernatant was subjected to insulin quantification using a homogeneous time-resolved fluorescence assay (HTRF) Insulin Ultrasensitive kit (Revvity, Waltham, MA, USA, Cat# 62IN2PEH) in accordance with the manufacturer's protocol.

3.11. Transfection small interfering RNAs (siRNAs) targeting *Khk* and *Aldob*

siRNAs targeting *Khk* (Dharmacon, Lafayette, CO, USA, Cat# M-062217-01-0005), *Aldob* (Cat# M-064045-00-0005), and non-targeting siRNA (Cat# D-001206-14-50) were reverse-transfected using the DharmaFECT 2 transfection reagent (Dharmacon, Lafayette, CO, USA, Cat# T-2002-03). A complex of siRNA (40 nM) and DharmaFECT 2 (0.4%) was prepared in serum-free DMEM (Sigma-Aldrich, St. Louis, MO, USA, Cat# D5796) in accordance with the manufacturer's instructions. For GLP-1 secretion measurements, siRNA/DharmaFECT 2 complex (100 μL/well) was combined with the cell suspension (0.75×10^6 cells/mL, 400 μL/well) and seeded in a 24-well plate pre-coated with 3% Matrigel (Corning, Glendale, AZ, USA, Cat# 356234). For RT-PCR, siRNA/DharmaFECT 2 complex (200 μL/well) was combined with the cell suspension (0.75×10^6 cells/mL, 800 μL/well) and seeded in a 12-well plate pre-coated with 3% Matrigel. For ATP/ADP ratio and Ca^{2+} measurements, the cells were seeded in a 35 mm glass-bottom dish (Matsunami Glass, Osaka, Japan, Cat# D11530H) pre-coated with 3% Matrigel at a density of 1.28×10^5 cells/dish. Following 1 h

incubation, the culture media was replaced with a mixture of siRNA/DharmaFECT 2 complex (400 μL/dish) and complete culture media (1.6 mL/dish). The subsequent experiments were conducted after a 48-hour culture period.

3.12. GLP-1 secretion from GLUTag cells

GLP-1 secretion from GLUTag cells was measured using the static incubation method. A 24-well plate (Corning, Glendale, AZ, USA, Cat# 353047) was pre-coated with 3% Matrigel (Corning, Glendale, AZ, USA, Cat# 356234). Cells were seeded at a density of 3×10^5 cells/well and cultured for 48 h. KRBH was supplemented with 10 μM sitagliptin phosphate (Tokyo Chemical Industry, Tokyo, Japan; CAS: 654671-78-0, Cat# I1231) to inhibit the degradation of active GLP-1. The cells were washed thrice with KRBH, followed by a pre-incubation period of 30 min with 300 μL/well KRBH. Subsequently, the supernatant was replaced with 300 μL/well of fresh KRBH containing the specified stimulations and incubated for 60 min at 37 °C. The reaction was terminated by cooling the plate on ice for ten minutes, after which the entire supernatant was collected for the quantification of released GLP-1 using the homogeneous time-resolved fluorescence assay (HTRF) active GLP-1 detection kit (Revvity, Waltham, MA, USA, Cat# 62 62GLPPEG) in accordance with the manufacturer's instructions. Fluorescence was measured using an Infinite F Nano+ microplate reader (Tecan, Zürich, Switzerland).

3.13. Imaging of intracellular Ca^{2+} in GLUTag cells

Imaging of intracellular Ca^{2+} was performed as previously described (Murao et al., 2024), with minor modifications. The cells were seeded in a 35 mm glass-bottom dish (Matsunami Glass, Osaka, Japan, Cat# D11530H) pre-coated with 3% Matrigel (Corning, Glendale, AZ, USA,Cat# 356234) at a density of 1.28×10^5 cells/dish and cultured for 48 h. Subsequently, the cells were loaded with 1 μM Fluo-4 AM (Dojindo, Kumamoto, Japan, Cat# F312) in KRBH supplemented with 0.04% Pluronic F-127 (Sigma-Aldrich, St. Louis, MO, USA, CAS: 9003-11-6, Cat# P2443-250G) for 20 min at 37 °C. Following brief washing, cells were loaded with 1 mL of KRBH, and basal recordings were performed for 300 s (from time -300 to 0). Immediately after the addition of 1 mL of KRBH supplemented with 20 mM fructose, recordings were resumed for another 1800 s. Time-lapse images were obtained using a Zeiss LSM 980 Airyscan2 inverted confocal laser scanning super-resolution

microscope equipped with a Plan Apo 40×, 1.4 Oil DICII objective lens (Carl Zeiss Microscopy, Jena, Germany). The cells were excited at 488 nm laser with 0.3% output power, and fluorescence emission was measured at 508-579 nm. During observation, the cells were maintained at 37 °C using an incubator XLmulti S2 DARK (Pecon, Erbach, Germany). Images were acquired in the frame mode at a rate of 2 frames per second and with an image size of 212.2 × 212.2 μm (512 × 512 pixels). The obtained images were analyzed using the ZEN 3.0 imaging software (Carl Zeiss Microscopy, Jena, Germany, RRID:SCR_021725). Cells were randomly chosen for analysis for each stimulation, and the number of cells analyzed is indicated in the figure legends. The fluorescence intensity of the entire cell body (F) was calculated and normalized to its average between -5 and 0 min (F0).

3.14. Imaging of intracellular ATP/ADP ratio in GLUTag cells

The cells were seeded in a 35 mm glass-bottom dish (Matsunami Glass, Osaka, Japan, Cat# D11530H) at a density of 1.28×10^5 cells/dish and cultured for 1 h. Subsequently, the cells were transfected with GW1-PercevalHR plasmid (0.1 μg/dish) or double transfection of GW1-PercevalHR and siRNAs using DharmaFECT 2 transfection reagent (Dharmacon, Lafayette, CO, USA, Cat# T-2002-03). Following a 48h culture, the cells were washed and loaded with 1 mL of fresh KRBH, and basal recordings were conducted for 300 s (from time -300 to 0). Immediately after the addition of 1 mL of KRBH supplemented with stimulations at 2× concentration, recordings were resumed for an additional 2400 s with a time interval of 5 s. The cells were excited at 445 nm and 488 nm laser with 0.8% and 0.3% output power, respectively, and fluorescence emission was measured at 508-543 nm. The ratio (R) of the fluorescence at 445 nm and 488 nm was calculated and normalized to the average fluorescence intensity between -300 and 0 s (R0). The remaining experimental configurations were identical to those described for Ca^{2+} imaging.

3.15. Quantitative reverse transcription polymerase chain reaction (RT-qPCR)

cDNA was prepared from GLUTag cells using CellAmp Direct Lysis and RT set (Takara Bio, Shiga, Japan, Cat# 3737S/A) according to the manufacturer's instructions. Quantitative real-time PCR was performed on a QuantStudio 7 Flex system (Thermo Fisher Scientific, Waltham, MA, USA, RRID:SCR_020245) using TaqMan Universal Master Mix II with UNG (Thermo Fisher Scientific, Waltham, MA, USA, Cat# 4440038) and Taqman probes: *Khk* (Cat# Mm00434647_m1), *Aldob* (Cat# Mm00523293_m1), and *Tbp* (Cat#

Mm01277042_m1). Relative gene expression was calculated using the $2^{-\Delta\Delta CT}$ method and normalized to *Tbp.*

3.16. Isolation of intestinal crypts from mice

The mice were fed standard chow and water until euthanasia via isoflurane exposure. Intestinal crypts were isolated from the distal half of the small intestine, including the jejunum and ileum, where fructose is absorbed (Bode et al., 1981). Isolation was conducted in accordance with established protocols, with minor modifications (Bas et al., 2014; O'Rourke et al., 2016). The distal half of the small intestine was longitudinally incised, rinsed with ice-cold phosphate-buffered saline (PBS), and sectioned into 5 mm segments using razors. The following procedure was conducted on ice. The intestinal fragments from two mice were combined in a 50 mL tube and dissociated into crypts through the following procedures: washing by vigorous pipetting in 10 mL PBS supplemented with 5 mM ethylenediaminetetraacetic acid (EDTA); digestion by gentle agitation in 10 mL 5 mM EDTA/PBS for 10 min; gentle agitation in 10 mL fresh 5 mM EDTA/PBS for an additional 30 min; gentle washing with 10 mL PBS; dispersion of crypts by vigorous pipetting with 10 mL PBS three times, with the supernatant combined; centrifugation at 300 × g for 5 min; the crypts were obtained as suspension after careful removal of the supernatant. The crypts isolated from two mice per genotype were combined and immediately utilized for subsequent metabolic labelling procedures. Fluorescent images were acquired using a BZ-X810 microscope (Keyence, Osaka, Japan, RRID:SCR_025160).

3.17. Fructose metabolic tracing in intestinal crypts

500 μL of the crypt suspension was aliquoted into 1.5 mL screw tubes and subsequently washed three times with 2.8 mM glucose-KRBH. The crypts were pre-incubated with 500 μL 2.8 mM glucose-KRBH for 60 min at 37 °C. Subsequently, 500 μL of 2.8 mM glucose-KRBH with or without 100 mM $^{13}C_6$-fructose (Cambridge Isotope Laboratories, Tewksbury, MA, USA, CAS: 287100-63-4, Cat# CLM-1553-1) was added to the reaction ($^{13}C_6$-fructose final concentration: 50 mM). The crypts were incubated for an additional 60 min at 37 °C. To facilitate ventilation, the tube lids were kept open during incubation. Following centrifugation at 500 × g for 1 min, the supernatant was discarded, the crypt pellet was rapidly lysed by the addition of 500 μL ice-cold extraction buffer (67.5% methanol, 7.5% chloroform, and 25%

water), and the entire tube was snap-frozen in liquid nitrogen. For extraction of the metabolites, samples were supplemented with 80 μL of diluted (1:640) internal standard (Human Metabolome Technologies, Yamagata, Japan, Cat# H3304-1002), 165 μL of methanol, and 465 μL of chloroform. The samples were then homogenized using a pre-cooled bead crusher at 3200 rpm for 1 min and centrifuged at 15000 × g at 4 °C for 3 min. The aqueous layer was transferred to pre-wetted ultrafiltration tubes (Human Metabolome Technologies, Yamagata, Japan, Cat# UFC3LCCNB-HMT) and centrifuged at 9100 × g, 4 °C until completely filtrated. The filtrate was freeze-dried, re-dissolved in 10 μL of water, and subjected to mass spectrometry. The organic layer was evaporated by decompression at room temperature, and the residue was resuspended in lysis buffer (see Section 4.7.), which was then subjected to a BCA protein assay (Thermo Fisher Scientific, Waltham, MA, USA, Cat# 23225).

The concentration of metabolites was measured using G7100A capillary electrophoresis (Agilent Technologies, Santa Clara, CA, USA) interfaced with a G6224A time-of-flight LC/MS mass spectrometer (Agilent Technologies, Santa Clara, CA, USA). A G1310A isocratic pump (Agilent Technologies, Santa Clara, CA, USA) equipped with a G1379B degasser (Agilent Technologies, Santa Clara, CA, USA) was used to supply sheath liquid (Human Metabolome Technologies, Yamagata, Japan, Cat# H3301-2020). The mass spectrometer was operated in the negative ionization mode. All separations were performed on fused silica capillaries (Human Metabolome Technologies, Yamagata, Japan, Cat# H3305-2002) at 25 °C using an anion analysis buffer (Human Metabolome Technologies, Yamagata, Japan, Cat# H3302-2021) as the background electrolyte. The applied voltage was set to 30 kV at 20 °C, together with a pressure of 15 mbar. Sheath liquid was delivered to a nebulizer by an isocratic pump at 1 mL/min. Chromatograms and mass spectra were analyzed by MassHunter qualitative analysis version 10.0 (Agilent Technologies, Santa Clara, CA, USA, RRID:SCR_015040). Annotation and quantification of chromatogram peaks were performed using a standard mixture (Human Metabolome Technologies, Yamagata, Japan, Cat# H3302-2021) and D-fructose 1-phosphate dipotassium salt (Santa Cruz Biotechnology, Dallas, TX, USA, CAS: 103213-47-4, Cat# sc-500907) as references.

3.18. Statistical Analysis

Sample sizes were estimated from the expected effect size based on previous experiments. No randomization or blinding was employed. Experiments were conducted multiple times on separate occasions using distinct cell passages or different mice, with N indicating the number of repetitions. Only representative results from these experiments are shown in the figures. For in vivo experiments, n represents the number of mice. For GLP-1 secretion, n represents the number of different wells under the same conditions. For insulin secretion from islets, n represents the number of wells, each containing five islets. For Ca^{2+} and ATP/ADP ratio measurements, n represents the number of different single cells analyzed, with data pooled from 2 to 3 independent measurements. For fructose metabolic tracing, n represents the number of samples aliquoted from crypts pooled from two mice per genotype. Data are presented as the mean ± standard deviation (SD) along with the plot of individual data points. For statistical comparisons between two groups, a two-tailed unpaired Welch's unpaired t-test was used. For comparisons between three groups, Welch's one-way analysis of variance (ANOVA) was followed by pairwise comparisons corrected using Dunnett's method. Normality of the distribution was confirmed by the Shapiro-Wilk test. P-values were indicated in the figures, with those less than 0.05 considered statistically significant. Statistical analyses are indicated in the figure legends. Statistical analyses were performed using GraphPad Prism 10 (Graphpad Software, Boston, MA, USA, https://www.graphpad.com; RRID:SCR_002798).

4. RESULTS

4.1. Short-term fructose ingestion increases plasma insulin levels in lean mice

To examine the metabolic impact of fructose in both lean and diabetic states, we used the NSY.B6-A^y mouse strain, a model of spontaneous obese diabetes. These strains were recently developed by introducing an obesity-associated agouti yellow (A^y) mutation in the agouti (a) gene into a diabetes-susceptible NSY background (Ohno et al., 2022). Male mice with the heterozygous (A^y/a) genotype exhibited obesity and elevated blood glucose levels, whereas their wild-type (a/a) counterparts remained lean (Supplementary Figure 1, A–B), which is consistent with previous findings (Ohno et al., 2022). Fructose administration was conducted as illustrated in Figure 1A.

Following the 24h administration period, A^y/a mice exhibited significant hyperglycemia and hyperinsulinemia compared to *a*/*a* mice, both without fructose (Figure 1, B–C). In *a*/*a* mice, fructose did not affect blood glucose (Figure 1B) but increased plasma insulin levels (Figure 1C). Conversely, in A^y/a mice, fructose increased blood glucose (Figure 1B) but did not alter plasma insulin levels (Figure 1C), indicating an inverse correlation between glycemia and insulin levels following fructose ingestion.

During oral glucose tolerance tests (OGTT), A^y/a mice exhibited impaired glucose tolerance (Figure 1, D–E) and hyperinsulinemia compared to *a*/*a* mice, both without fructose (Figure 1, F–G). In *a*/*a* mice, fructose ingestion resulted in improved glucose tolerance (Figure 1, D–E), accompanied by elevated insulin levels persisting after glucose administration (Figure 1, F–G). Conversely, in A^y/a mice, fructose ingestion did not elicit any significant differences in glucose tolerance or insulin levels (Figure 1, D–G). In intraperitoneal insulin tolerance tests, A^y/a mice exhibited severe insulin resistance, with fructose having no effect on either strain (Supplementary Figure 1, C–D). These results suggest that improved glucose tolerance is primarily attributable to an enhanced insulin response.

These findings highlight the differential metabolic responses following fructose ingestion under lean and diabetic conditions: fructose-induced insulin response may help maintain normal glycemia and enhance glucose tolerance in lean mice, whereas these effects were abolished in diabetic mice.

4.2. GLP-1 is required for fructose-induced insulin response

We investigated circulating fructose and fructose-stimulated insulinotropic hormone levels as potential factors stimulating fructose-induced insulin secretion in vivo.

Fructose enhances glucose-induced insulin secretion from β-cells in vitro at high concentrations (3–27 mM) (Grodsky et al. 1963; Zawalich et al. 1977; Grant et al. 1980; Kyriazis et al. 2012; Bartley et al. 2019; Murao et al. 2025). To assess whether plasma fructose levels attained these concentrations under our conditions, fructose in the tail and portal veins was quantified using liquid chromatography-tandem mass spectrometry (LC-MS/MS). Without fructose administration, fructose concentrations were approximately 5 μM in both veins. However, fructose ingestion elevated the concentrations to 100–200 μM and

10–20 μM in the tail and portal veins, respectively (Figure 2, A–B). The levels of fructose in the portal vein were lower and exhibited greater variability than those in the tail veins. This is likely due to the random timing of fructose consumption followed by its swift removal from the portal blood (Jang et al., 2018). We also tested the acute gavage of 2 g/kg fructose to *a*/*a*, A^y/*a*, and C57BL/6J (B6) mice (Supplementary Figure 2, A–B). Plasma fructose levels reached their highest point (~100 μM) between 15 and 30 min, returning to initial levels within 120 min, indicating that the maximum plasma fructose level was approximately 100 μM. Nevertheless, our recent findings showed that fructose concentrations below 3 mM failed to affect GIIS in *a*/*a* mouse islets (Murao et al., 2025). The difference between these concentrations does not support the notion that circulating fructose directly stimulates β-cells.

Therefore, our investigation focused on insulinotropic hormones, including GLP-1, GIP, and glucagon. In the fasting state without fructose, A^y/*a* mice exhibited elevated GLP-1 and GIP levels compared to *a*/*a* mice (Figure 2, C–D). Fructose administration significantly increased GLP-1 and GIP levels in both *a*/*a* and A^y/*a* mice (Figure 2, C–D). Glucagon levels remained unaltered by fructose (Supplementary Figure 2C). Interestingly, exendin [9-39], a GLP-1 receptor antagonist, cancelled the increase in insulin levels following fructose ingestion in *a*/*a* mice (Figure 2E), suggesting that GLP-1 is essential for the insulinotropic effect of fructose. In contrast, fructose administration to A^y/*a* mice did not affect insulin levels, despite a significant increase in GLP-1 and GIP levels. Consistent with this, GLP-1 and GIP effectively potentiated insulin secretion in isolated *a*/*a* mouse islets, but failed to do so in A^y/*a* mouse islets (Figure 2, E–F). Consequently, the absence of a fructose-induced insulin response in A^y/*a* mice is likely attributable to the unresponsiveness of β-cells to GLP-1 and GIP.

To better understand the roles of GLP-1 and GIP in fructose-induced insulin response, we studied B6 mice, glucagon knockout mice (*Gcg*-/-) (Hayashi et al., 2009), and GIP receptor knockout mice (*Gipr*-/-) (Miyawaki et al., 1999). Initially, in B6 mice, fructose administration led to a slight, non-significant increase in blood glucose levels (Figure 3A), accompanied by increases in insulin, GLP-1, and GIP levels (Figure 3, B–D). Next, *Gcg*-/- mice, which lack proglucagon-derived peptides such as GLP-1 and glucagon due to a *gfp* insertion disrupting the proglucagon gene (Hayashi et al., 2009), showed significantly higher blood glucose levels after fructose administration (Figure 3E), while insulin and GIP levels remained unchanged (Figure 3, F–G). These findings suggest that the insulin response to

fructose is defective when both GLP-1 and GIP responses are absent, although the reason for the lack of a GIP response in *Gcg*-/- mice is not clear. Lastly, *Gipr*-/- mice exhibited fructose-induced increases in insulin, GLP-1, and GIP levels (Figure 3, I–K), with a moderate rise in blood glucose levels (Figure 3H), phenocopying B6 mice. Thus, the insulin response to fructose remains intact, even without the GIP response. Collectively, these findings suggest that GIP is nonessential, whereas GLP-1 is required for the fructose-induced insulin response. This observation aligns with the exendin [9-39] result (Figure 2E).

4.3. GLP-1 secretion is coupled to intracellular fructose metabolism

We explored the mechanisms by which ingested fructose enhanced GLP-1 secretion. Earlier studies have suggested mechanisms similar to GIIS: fructose metabolism produces ATP in L-cells, causing K_{ATP} channels to close, which leads to membrane depolarization and subsequent Ca^{2+} entry (Kuhre et al., 2014; Gribble et al., 2003). This theory is supported by several GLUTag cell experiments, but further validation is warranted, as noted in the Discussion section. Our aim was to confirm whether fructose metabolism increases the ATP/ADP ratio, promotes Ca^{2+} influx, and stimulates GLP-1 secretion.

Fructose dose-dependently enhanced GLP-1 secretion at concentrations above 10 mM (Figure 4A). To investigate the involvement of fructose metabolism, we used siRNA to knock down two key enzymes involved in fructolysis, ketohexokinase (*Khk*) and aldorase B (*Aldob*) (Supplementary Figure 3, A–B). Intracellular ATP/ADP ratio and calcium ($[Ca^{2+}]i$) were visualized using a Perceval HR biosensor (Tantama et al., 2013) and Fluo-4, respectively. Fructose triggered a gradual increase in the ATP/ADP ratio in control cells treated with non-targeting siRNA (siNT). This elevation was inhibited when *Khk* and *Aldob* were depleted (Figure 4, B–C, Supplementary Figure 3, C–D). Similarly, fructose triggered a gradual increase in $[Ca^{2+}]$ i with successive firing in siNT cells (Figure 4D). Knockdown of *Khk* and *Aldob* inhibited $[Ca^{2+}]i$ firing (Figure 4D) and reduced average $[Ca^{2+}]i$ responses (Supplementary Figure 3E), as quantified by the incremental area under the curve (iAUC) (Supplementary Figure 3F). Interestingly, both the ATP/ADP ratio and $[Ca^{2+}]i$ exhibited similar time-dependent trends, initially experiencing a transient decline upon fructose stimulation, followed by a steady rise. The initial decline might be attributed to swift ATP utilization by KHK, as previously observed in enterocytes (Merino et al., 2019), whereas the subsequent increase could be linked to ATP replenishment through fructose catabolism.

Finally, these knockdown cells exhibited impaired fructose-induced GLP-1 secretion (Figure 4E). These findings indicate that the suppression of fructose metabolism led to a decrease in the ATP/ADP ratio, $[Ca^{2+}]i$ response, and GLP-1 secretion. Research has shown that TEPP-46, an activator of pyruvate kinase M2 (PKM2), enhances fructose metabolism in both intestinal epithelial cells (Taylor et al., 2021) and β-cells (Murao et al., 2025). These findings prompted us to use TEPP-46 to further confirm the link between metabolism and secretion. In GLUTag cells, TEPP-46 significantly enhanced fructose-induced elevation of the ATP/ADP ratio (Figure 4F, Supplementary Figure 3G) and GLP-1 secretion (Figure 4G). Fructose-induced $[Ca^{2+}]i$ response and GLP-1 secretion were suppressed by nifedipine, an inhibitor of L-type voltage-dependent Ca^{2+} channels (VDCCs) (Figure 4, G–H), indicating that Ca^{2+} influx through L-type VDCC plays a permissive role in fructose-induced GLP-1 secretion. Collectively, these findings demonstrate that fructose metabolism increases the ATP/ADP ratio, which is positively correlated with $[Ca^{2+}]i$ and GLP-1 secretion.

4.4. Functional K_{ATP} channels are required for Fructose-induced GLP-1 secretion in vivo

To validate the involvement of K_{ATP} channels in fructose-induced GLP-1 secretion in vivo, we utilized *Kcnj11*$^{-/-}$ mice, which lack K_{ATP} channel activity throughout the body due to the disruption of the pore-forming subunit KCNJ11 (Miki et al., 1998). As anticipated, *Kcnj11*$^{-/-}$ mice exhibited null fructose-induced insulin and GLP-1 responses (Figure 5, B–C), resulting in a significant increase in glycemia (Figure 5A). Furthermore, administration of diazoxide, a K_{ATP} channel opener, inhibited the fructose-induced increase in GLP-1, but not GIP, in *a*/*a* mice (Figure 5, E–F). These findings demonstrate that fructose-induced GLP-1 secretion is dependent on functional K_{ATP} channels in vivo.

4.5. Characterization of Fructose metabolism in lean and diabetic mouse intestinal crypts

GLP-1 levels were higher in A^y/a mice than in *a*/*a* mice at baseline, and were further increased by fructose in both strains (Figure 2C). We examined whether these changes were determined by the metabolic conditions of the L-cells. Purified L-cells were technically unsuitable for metabolomic analysis owing to the scarcity of these cells after sorting. As an alternative strategy, we used isolated intestinal crypts.

The presence of L-cells was verified using *Gcg*$^{gfp/+}$ mouse crypts, where L-cells were labelled with GFP (Supplementary Figure 4A). Crypts from *a*/*a* and A^y/*a* mice were exposed to 50 mM $^{13}C_6$-fructose, a stable isotopomer in which all six carbon atoms are ^{13}C. The potential metabolic pathways of $^{13}C_6$-fructose are shown in Figure 6A. Isotopomers with 0-6 carbon atoms substituted by ^{13}C are denoted as M-M6. Naturally occurring isotopomers are represented by M and M1. The $^{13}C_6$-fructose can be metabolized into M6 F1P (fructose 1-phosphate), M3 GA3P (glyceraldehyde 3-phosphate), and M3 DHAP (dihydroxyacetone phosphate). Subsequently, M3 GA3P enters glycolysis and the TCA cycle, resulting in the formation of M2–M4 malate and M2–M6 citrate. These metabolites contribute to ATP generation through oxidative phosphorylation (OXPHOS). Another metabolic route for M3 GA3P is conversion to M3 lactate, which produces ATP. Additionally, M3 GA3P and M3 DHAP can be utilized in gluconeogenic processes to synthesize M6 G6P.

Figures 6B–6I show the quantity of $^{13}C_6$-Fru-derived isotopomers in *a*/*a* and A^y/*a* mouse crypts in the presence or absence of $^{13}C_6$-Fru. As anticipated, these isotopomers were detected in stimulated ($^{13}C_6$-Fru +) crypts but not in unstimulated ($^{13}C_6$-Fru -) crypts. $^{13}C_6$-Fru-derived isotopomers, with the exception of citrate [M2–M6], were observed at higher levels in $^{13}C_6$-Fru + A^y/*a* crypts compared to $^{13}C_6$-Fru + *a*/*a* crypts, suggesting increased fructolysis activity in A^y/*a* mouse crypts. Figures 6J–6 L indicate the quantity of unlabelled ATP and ADP and their ratio in the crypts. In the absence of $^{13}C_6$-Fru, ATP levels were elevated and ADP levels were reduced, resulting in an increased ATP/ADP ratio in A^y/*a* crypts compared to *a*/*a* crypts. ATP levels and the ATP/ADP ratio were further increased by $^{13}C_6$-Fru stimulation in both genotypes. These trends in ATP and ATP/ADP ratio were consistent with the differential GLP-1 levels in basal and fructose-stimulated states (Figure 2C), suggesting that the metabolic status of the intestine is reflected in fructose-induced GLP-1 secretion in vivo.

5. DISCUSSION

It has been previously documented that fructose stimulates GLP-1 and insulin secretion. The present study contextualized these hormonal responses and delineated the mechanism linking short-term fructose consumption and glycemia. We demonstrated that fructose stimulates GLP-1 secretion via intestinal fructose metabolism and K_{ATP} channels. GLP-1 subsequently induces a plasma insulin response, thereby suppressing hyperglycemia.

Research has shown that acute fructose consumption elevates blood glucose levels (Kuhre et al., 2014; Seino et al., 2015; Kong et al., 1999), potentially owing to fructose-to-glucose conversion in the intestine (Ockerman and Lundborg, 1965; Jang et al., 2018). This observation led researchers to hypothesize that fructose-induced insulin response is solely a result of a concurrent increase in glycemia. However, this hypothesis was challenged by the observed insulin response in *a*/*a* mice without a corresponding change in blood glucose levels (Figure 1, B–C). Importantly, our findings revealed that fructose-induced hyperglycemia was more pronounced in strains lacking a fructose-induced insulin response (increase in glycemia due to fructose [ΔBG], A^y/a: 80.17; $Gcg^{-/-}$: 64.78; $Kcnj11^{-/-}$: 93.93) than in other strains (ΔBG, *a*/*a*: 12.30; B6:30.58; $Gipr^{-/-}$: 26.62). These findings indicate that the fructose-induced insulin response is crucial for preventing hyperglycemia following fructose ingestion.

As a potential mechanism for fructose-induced insulin response, in vitro studies have demonstrated that high concentrations (>10 mM) of fructose can directly potentiate GIIS (Grodsky et al., 1963; Ashcroft et al., 1972; Zawalich et al., 1977; Grant et al., 1980; Murao et al., 2025). However, these effects have not been substantiated in vivo, likely because plasma fructose levels fall far below the concentration required for the direct stimulation of β-cells. Indeed, the observed plasma fructose levels (~100 μM) were in good agreement with previous measurements using 20% fructose diet-fed B6 mice (Patel et al., 2015) and sucrose-administered Wistar rats (Sugimoto et al., 2010). Human plasma fructose levels are also reported to be below 100 μM in the postprandial state (Kawasaki et al., 2004).

Glucose induces depolarizing currents in L-cells via two mechanisms: (1) SGLT-mediated Na^+/glucose transport and (2) GLUT2-mediated glucose uptake and intracellular metabolism, leading to K_{ATP} channel closure (Reimann et al., 2008; Kuhre et al., 2015; Hjørne et al., 2022). Both mechanisms lead to Ca^{2+} influx through VDCCs, which was demonstrated through its inhibition by nifedipine in GLUTag cells (Reimann et al., 2005), perfused rat intestine (Kuhre et al., 2015), and human intestine fragments (Sun et al., 2017).

As fructose is not a substrate for SGLT1 (Koepsell, 2020), it has been speculated that fructose-induced GLP-1 secretion relies solely on intracellular fructose metabolism and K_{ATP} channel closure. This hypothesis has been corroborated by several findings derived from GLUTag cells, including fructose-induced K_{ATP} channel closure and action potentials (Gribble et al., 2003), fructose-induced increase in intracellular NADPH levels (Kuhre et al.,

2014), and inhibition of fructose-induced GLP-1 secretion by diazoxide (Kuhre et al., 2014). However, prior studies lacked evidence regarding whether fructose metabolism elevates the ATP/ADP ratio and $[Ca^{2+}]i$, which we demonstrated in GLUTag cells (Figure 4). Additionally, the link between fructolysis activity, ATP/ADP ratio, and K_{ATP} channels was validated both in vivo and ex vivo in *Kcnj11*$^{-/-}$ mice (Figure 5) and intestinal crypts (Figure 6), suggesting that these results are not limited to a specific cell line. In contrast to the current study, our previous research showed that a substantial GLP-1 response occurs even in *Kcnj11*$^{-/-}$ mice 15 min after gavage with excess fructose (6 g/kg) (Seino et al., 2015). Potentially, fructose-induced GLP-1 response involves distinct mechanisms in the acute and subacute phases, with the former being at least partially independent of fructose metabolism. Given the substantial volume of liquid administered, mechanical stimuli may contribute to acute GLP-1 responses (Huang et al., 2024).

The effect of fructose ingestion on GIP secretion has been less extensively investigated than that of GLP-1. Fructose can enhance GIP secretion from primary-cultured K-cells (Parker et al., 2009). Consistently, the present study demonstrated that 24-h fructose ingestion robustly increased GIP levels across multiple strains. In contrast, research has shown that acute fructose administration failed to elevate GIP levels in normal mice, rats, and healthy humans (Kuhre et al., 2014). We previously observed that acute fructose ingestion can elicit a GIP response in streptozotocin-induced diabetic mice, but not in normal mice (Seino et al., 2015). These highly variable outcomes suggest that fructose-induced GIP secretion is sensitive to ingestion conditions and metabolic status. Notably, the impaired GIP response in *Kcnj11*$^{-/-}$ mice (Figure 5D) indicates that K_{ATP} channels are, at least in part, involved in fructose-induced GIP secretion, consistent with the abundant expression of K_{ATP} channel subunits in primary K-cells (Parker et al., 2009). Unexpectedly, fructose-induced GIP response was also deficient in *Gcg*$^{-/-}$ mice, with elevated basal GIP levels in the absence of fructose (compare Figure 3, G and K). Although the precise mechanism remains unknown, GLP-1 deficiency may alter K-cell function, leading to compensatory hypersecretion of GIP, as previously suggested (Iida et al., 2016). The mechanism underlying fructose-induced GIP secretion warrants further investigation.

In relation to daily life or clinical situations, our 24-hour ad-lib fructose ingestion is more physiologically relevant than the often-used gavage of excess doses, recapitulating the consumption of sugar-sweetened beverages (SSBs). SSBs are a major source of fructose in

contemporary diets containing 5–10% fructose (Ando et al., 2023) and are particularly detrimental to glycemic control (Stanhope et al., 2009; Imamura et al. 2016; Choo et al. 2018; Drouin-Chartier et al. 2019). Nevertheless, in a healthy state, the acute effect of dietary fructose on glycemia may be attenuated by the GLP-1/β-cell axis, as indicated by our observations in lean mice.

An important limitation of our study is that it did not address the potential long-term effects of fructose consumption. Evidence demonstrates that prolonged fructose intake, typically lasting more than 5 days, leads to obesity-associated phenotypes such as adiposity, hepatic insulin resistance, and hyperinsulinemia (Blakely et al., 1981; Basciano et al., 2005; Ter Horst et al., 2018; Hannou et al., 2018). Interestingly, a clinical study demonstrated that GLP-1 and insulin responses following fructose ingestion are more exaggerated in obese subjects than in healthy subjects (Galderisi et al., 2019). The increased fructose-induced GLP-1 response may reflect increased intestinal fructolysis, as observed in the intestinal crypts of A^y/a mice (Figure 6). As a potential explanation for obesity-related metabolic alterations in the intestine, studies have reported that GLUT5 and KHK are upregulated by high-fructose-high-sucrose diet consumption in the mouse intestine (Taylor et al., 2021).

Taken together, we propose the following roles for the GLP-1/β-cell axis in the development of fructose-associated metabolic syndrome. In a healthy state, the GLP-1/β-cell axis effectively counteracts the acute hyperglycemic effect of fructose. Subsequently, increased fructose consumption (i.e., habitual SSB intake), either independently or by promoting obesity, upregulates the GLP-1/β-cell axis, leading to chronic hyperinsulinemia, which further exacerbates obesity and insulin resistance. Under diabetic conditions, the detrimental glycemic impact of fructose becomes evident owing to the defective GLP-1/β-cell axis, which no longer mitigates the acute hyperglycemic effect of fructose. Notably, the impaired glycemic response to fructose may be attributed to β-cell unresponsiveness to GLP-1 rather than impaired fructose-induced GLP-1 secretion, as indicated by the A^y/a mouse results. This hypothesis aligns with clinical observations regarding meal ingestion in general (Yabe et al., 2015). The hypothesized significance of the GLP-1/β-cell axis in chronic fructose consumption requires further experimental validation.

Another limitation of this study was the use of intestinal crypts instead of purified L-cells for metabolic analysis. Although various methodologies are available to study L-cells (Kuhre

et al., 2021), reliable metabolomic data for L-cells are still lacking. Such an analysis may have been impeded by the difficulty in obtaining a sufficient number of sorted L-cells and by the disruption of the metabolic activity of L-cells through a cell sorting process. One advantage of our approach of maintaining the L-cell resident niche is to preserve L-cell metabolism close to its in situ status. However, the extent to which these results reflect the specific metabolic activity in L-cells remains to be validated. Future technical advancements are warranted for the precise characterization of L-cell metabolism.

In conclusion, this study identified the intestinal fructose metabolism/GLP-1/β-cell axis as a counter-regulatory mechanism for glycemia following short-term fructose ingestion. These findings provide significant insights into the understanding of systemic fructose metabolism.

6. AUTHOR CONTRIBUTIONS

Conceptualization, N.M.; Methodology, N.M..; Investigation, N.M., R.M., T.H., S.S., E.T., and M.H.; Resources: T.O., N.Y., N.H., and Y.H.; Writing – Original Draft: N.M.; Writing – Review & Editing: N.M., Y.S., Y.Y., Y.H., and A.S.; Data Curation: N.M.; Visualization: N.M.; Supervision: Y.S., Y.Y., and A.S.; Funding Acquisition: N.M.

7. ACKNOWLEDGEMENTS

The authors are grateful to President Yutaka Seino (Kansai Electric Power Hospital) for his generous support in this research. The authors thank Professor Daniel Drucker and Dr. Akira Hirasawa for GLUTag cells; Yoshikazu Hoshino (Hoshino Laboratory Animals, Inc) for NSY.B6 mice; Yasuhiro Maeda (Fujita Health University) for assistance with LC-MS. The authors thank Asami Yamaguchi and Megumi Akiyama for their excellent technical assistance.

8. DATA AVAILABILITY

Data supporting the findings of this study are available from the corresponding author upon reasonable request.

9. FUNDING

This study was supported by JSPS KAKENHI Grant Numbers JP22K20869 and JP23K15401 for N.M. Research grants for N.M. were provided by the Japan Association for

Diabetes Education and Care, Daiwa Securities Foundation, Suzuken Memorial Foundation, Japan Diabetes Foundation, The Hori Sciences and Arts Foundation, Manpei Suzuki Diabetes Foundation, and Fujita Academy.

10. CONFLICT OF INTEREST

The authors declare no conflict of interest.

11. REFERENCES

1. Ahrén, B., Yamada, Y., and Seino, Y. (2021) The insulin response to oral glucose in GIP and GLP-1 receptor knockout mice: Review of the literature and stepwise glucose dose response studies in female mice. *Frontiers in endocrinology* **12**, 665537

2. Ando, Y., Ohta, Y., Munetsuna, E., Yamada, H., Nouchi, Y., Kageyama, I., Mizuno, G., Yamazaki, M., Fujii, R., and Ishikawa, H. (2023) Laboratory analysis of glucose, fructose, and sucrose contents in Japanese common beverages for the exact assessment of beverage-derived sugar intake. *Fujita Medical Journal* **9**, 126-133

3. Ashcroft, S. J., Bassett, J. M., and Randle, P. J. (1972) Insulin secretion mechanisms and glucose metabolism in isolated islets. *Diabetes* **21**, 538-545

4. Bartley, C., Brun, T., Oberhauser, L., Grimaldi, M., Molica, F., Kwak, B. R., Bosco, D., Chanson, M., and Maechler, P. (2019) Chronic fructose renders pancreatic β-cells hyper-responsive to glucose-stimulated insulin secretion through extracellular ATP signaling. *American Journal of Physiology-Endocrinology and Metabolism* **317**, E25-E41

5. Bas, T., and Augenlicht, L. H. (2014) Real time analysis of metabolic profile in ex vivo mouse intestinal crypt organoid cultures. *Journal of Visualized Experiments: JoVE*, 52026

6. Basciano, H., Federico, L., and Adeli, K. (2005) Fructose, insulin resistance, and metabolic dyslipidemia. *Nutrition & metabolism* **2**, 1-14

7. Blakely, S. R., Hallfrisch, J., Reiser, S., and Prather, E. S. (1981) Long-term effects of moderate fructose feeding on glucose tolerance parameters in rats. *The Journal of nutrition* **111**, 307-314

8. Bode, C., Eisenhardt, J., Haberich, F., and Bode, J. C. (1981) Influence of feeding fructose on fructose and glucose absorption in rat jejunum and ileum. *Research in Experimental Medicine* **179**, 163-168

9. Choo, V. L., Viguiliouk, E., Mejia, S. B., Cozma, A. I., Khan, T. A., Ha, V., Wolever, T. M., Leiter, L. A., Vuksan, V., and Kendall, C. W. (2018) Food sources of fructose-containing sugars and glycaemic control: systematic review and meta-analysis of controlled intervention studies. *bmj* **363**

10. Drouin-Chartier, J.-P., Zheng, Y., Li, Y., Malik, V., Pan, A., Bhupathiraju, S. N., Tobias,

D. K., Manson, J. E., Willett, W. C., and Hu, F. B. (2019) Changes in consumption of sugary beverages and artificially sweetened beverages and subsequent risk of type 2 diabetes: results from three large prospective US cohorts of women and men. *Diabetes care* **42**, 2181-2189

11. Drucker, D. J., Jin, T., Asa, S. L., Young, T. A., and Brubaker, P. L. (1994) Activation of proglucagon gene transcription by protein kinase-A in a novel mouse enteroendocrine cell line. *Molecular endocrinology* **8**, 1646-1655

12. Galderisi, A., Giannini, C., Van Name, M., and Caprio, S. (2019) Fructose Consumption Contributes to Hyperinsulinemia in Adolescents With Obesity Through a GLP-1–Mediated Mechanism. *The Journal of Clinical Endocrinology & Metabolism* **104**, 3481-3490

13. Grant, A., Christie, M., and Ashcroft, S. (1980) Insulin release from human pancreatic islets in vitro. *Diabetologia* **19**, 114-117

14. Gribble, F. M., Williams, L., Simpson, A. K., and Reimann, F. (2003) A novel glucose-sensing mechanism contributing to glucagon-like peptide-1 secretion from the GLUTag cell line. *Diabetes* **52**, 1147-1154

15. Grodsky, G. M., Batts, A. A., Bennett, L. L., Vcella, C., McWilliams, N. B., and Smith, D. F. (1963) Effects of carbohydrates on secretion of insulin from isolated rat pancreas. *American Journal of Physiology-Legacy Content* **205**, 638-644

16. Hannou, S. A., Haslam, D. E., McKeown, N. M., and Herman, M. A. (2018) Fructose metabolism and metabolic disease. *The Journal of clinical investigation* **128**, 545-555

17. Hansotia T, Baggio LL, Delmeire D, Hinke SA, Yamada Y, Tsukiyama K, Seino Y, Holst JJ, Schuit F, and Drucker DJ. (2004) Double incretin receptor knockout (DIRKO) mice reveal an essential role for the enteroinsular axis in transducing the glucoregulatory actions of DPP-IV inhibitors. *Diabetes* **53**, 1326-1235

18. Hayashi, Y., Yamamoto, M., Mizoguchi, H., Watanabe, C., Ito, R., Yamamoto, S., Sun, X.-y., and Murata, Y. (2009) Mice deficient for glucagon gene-derived peptides display normoglycemia and hyperplasia of islet α-cells but not of intestinal L-cells. *Molecular endocrinology* **23**, 1990-1999

19. Henquin, J.-C. (2000) Triggering and amplifying pathways of regulation of insulin secretion by glucose. *Diabetes* **49**, 1751-1760

20. Henquin, J.-C. (2009) Regulation of insulin secretion: a matter of phase control and amplitude modulation. *Diabetologia* **52**, 739-751

21. Hjørne, A. P., Modvig, I. M., and Holst, J. J. (2022) The sensory mechanisms of nutrient-induced GLP-1 secretion. *Metabolites* **12**, 420

22. Holst, J. J., and Gromada, J. (2004) Role of incretin hormones in the regulation of insulin secretion in diabetic and nondiabetic humans. *American Journal of Physiology-Endocrinology And Metabolism* **287**, E199-E206

23. Huang, Y., Mo, H., Yang, J., Gao, L., Tao, T., Shu, Q., Guo, W., Zhao, Y., Lyu, J., and Wang, Q. (2024) Mechano-regulation of GLP-1 production by Piezo1 in intestinal L cells. *eLife* **13**, RP97854

24. Iida, A., Seino, Y., Fukami, A., Maekawa, R., Yabe, D., Shimizu, S., Kinoshita, K., Takagi, Y., Izumoto, T., and Ogata, H. (2016) Endogenous GIP ameliorates impairment of insulin secretion in proglucagon-deficient mice under moderate beta cell damage induced by streptozotocin. *Diabetologia* **59**, 1533-1541

25. Imamura, F., O'Connor, L., Ye, Z., Mursu, J., Hayashino, Y., Bhupathiraju, S. N., and Forouhi, N. G. (2015) Consumption of sugar sweetened beverages, artificially sweetened beverages, and fruit juice and incidence of type 2 diabetes: systematic review, meta-analysis, and estimation of population attributable fraction. *Bmj* **351**

26. Iwasaki, M., Minami, K., Shibasaki, T., Miki, T., Miyazaki, J., and Seino, S. (2010) Establishment of new clonal pancreatic β□cell lines (MIN6□K) useful for study of incretin/cyclic adenosine monophosphate signaling. *Journal of Diabetes Investigation* **1**, 137-142

27. Jang, C., Hui, S., Lu, W., Cowan, A. J., Morscher, R. J., Lee, G., Liu, W., Tesz, G. J., Birnbaum, M. J., and Rabinowitz, J. D. (2018) The small intestine converts dietary fructose into glucose and organic acids. *Cell metabolism* **27**, 351-361. e353

28. Kagiyama, N., Ikeda, T., and Nomura, T. (2006) Japanese Guidelines and regulations for scientific and ethical animal experimentation. In *In Vivo Models of Inflammation: Volume I* pp. 187-191, Springer

29. Kawasaki, T., Ogata, N., Akanuma, H., Sakai, T., Watanabe, H., Ichiyanagi, K., and Yamanouchi, T. (2004) Postprandial plasma fructose level is associated with retinopathy in patients with type 2 diabetes. *Metabolism* **53**, 583-588

30. Koepsell, H. (2020) Glucose transporters in the small intestine in health and disease. *Pflügers Archiv-European Journal of Physiology* **472**, 1207-1248

31. Kong, M.-F., Chapman, I., Goble, E., Wishart, J., Wittert, G., Morris, H., and Horowitz, M. (1999) Effects of oral fructose and glucose on plasma GLP-1 and appetite in normal subjects. *Peptides* **20**, 545-551

32. Kuhre, R. E., Deacon, C. F., Holst, J. J., and Petersen, N. (2021) What is an L-cell and how do we study the secretory mechanisms of the L-cell? *Frontiers in Endocrinology* **12**, 694284

33. Kuhre, R. E., Frost, C. R., Svendsen, B., and Holst, J. J. (2015) Molecular mechanisms of glucose-stimulated GLP-1 secretion from perfused rat small intestine. *Diabetes* **64**, 370-382

34. Kuhre, R. E., Gribble, F. M., Hartmann, B., Reimann, F., Windeløv, J. A., Rehfeld, J. F., and Holst, J. J. (2014) Fructose stimulates GLP-1 but not GIP secretion in mice, rats, and humans. *American Journal of Physiology-Gastrointestinal and Liver Physiology* **306**, G622-G630

35. Kyriazis, G. A., Soundarapandian, M. M., and Tyrberg, B. (2012) Sweet taste receptor signaling in beta cells mediates fructose-induced potentiation of glucose-stimulated insulin secretion. *Proceedings of the National Academy of Sciences* **109**, E524-E532

36. Larke, J. A., Bacalzo, N., Castillo, J. J., Couture, G., Chen, Y., Xue, Z., Alkan, Z., Kable, M. E., Lebrilla, C. B., and Stephensen, C. B. (2023) Dietary intake of monosaccharides from foods is associated with characteristics of the gut microbiota and gastrointestinal inflammation in healthy US adults. *The Journal of Nutrition* **153**, 106-119

37. Merino, B., Fernández-Díaz, C. M., Cózar-Castellano, I., and Perdomo, G. (2019) Intestinal fructose and glucose metabolism in health and disease. *Nutrients* **12**, 94.

38. Miki, T., Nagashima, K., Tashiro, F., Kotake, K., Yoshitomi, H., Tamamoto, A., Gonoi, T., Iwanaga, T., Miyazaki, J., and Seino, S. (1998) Defective insulin secretion and enhanced insulin action in KATP channel-deficient mice. *Proceedings of the National Academy of Sciences* **95**, 10402-10406

39. Miyawaki, K., Yamada, Y., Yano, H., Niwa, H., Ban, N., Ihara, Y., Kubota, A., Fujimoto, S., Kajikawa, M., and Kuroe, A. (1999) Glucose intolerance caused by a defect in the entero-insular axis: a study in gastric inhibitory polypeptide receptor knockout mice. *Proceedings of the National Academy of Sciences* **96**, 14843-14847

40. Murao, N., Morikawa, R., Seino, Y., Shimomura, K., Maejima, Y., Ohno, T., Yokoi, N., Yamada, Y., and Suzuki, A. (2025) Pyruvate kinase modulates the link between β-cell fructose metabolism and insulin secretion. *The FASEB Journal*. 2025; 39:e70500.

41. Murao, N., Morikawa, R., Seino, Y., Shimomura, K., Maejima, Y., Yamada, Y., and Suzuki, A. (2024) Sildenafil amplifies calcium influx and insulin secretion in pancreatic β cells. *Physiological Reports* **12**, e16091

42. Murao, N., Yokoi, N., Takahashi, H., Hayami, T., Minami, Y., and Seino, S. (2022) Increased glycolysis affects β-cell function and identity in aging and diabetes. *Molecular metabolism* **55**, 101414

43. Nauck, M. A., and Meier, J. J. (2016) The incretin effect in healthy individuals and those with type 2 diabetes: physiology, pathophysiology, and response to therapeutic interventions. *The lancet Diabetes & endocrinology* **4**, 525-536

44. Nauck, M., Stöckmann, F., Ebert, R., and Creutzfeldt, W. (1986) Reduced incretin effect in type 2 (non-insulin-dependent) diabetes. *Diabetologia* **29**, 46-52

45. Ockerman, P., and Lundborg, H. (1965) Conversion of fructose to glucose by human jejunum. Absence of galactose-to-glucose conversion.

46. Ohno, T., Miyasaka, Y., Yoshida, K., Kobayashi, M., Horio, F., Yokoi, N., Mizuno, M., and Ikegami, H. (2022) A novel model mouse for type 2 diabetes mellitus with early onset and persistent hyperglycemia. *Experimental Animals* **71**, 510-518

47. O'Rourke, K. P., Ackerman, S., Dow, L. E., and Lowe, S. W. (2016) Isolation, culture, and maintenance of mouse intestinal stem cells. *Bio-protocol* **6**, e1733-e1733

48. Parker, H., Habib, A., Rogers, G., Gribble, F., and Reimann, F. (2009) Nutrient-dependent secretion of glucose-dependent insulinotropic polypeptide from primary murine K cells. *Diabetologia* **52**, 289-298

49. Patel, C., Sugimoto, K., Douard, V., Shah, A., Inui, H., Yamanouchi, T., and Ferraris, R. P. (2015) Effect of dietary fructose on portal and systemic serum fructose levels in rats and in KHK−/− and GLUT5−/− mice. *American Journal of Physiology-Gastrointestinal and Liver Physiology* **309**, G779-G790

50. Pepin, A., Stanhope, K. L., and Imbeault, P. (2019) Are Fruit Juices Healthier Than Sugar-Sweetened Beverages? A Review. *Nutrients*, **11**, 1006

51. Preitner, F., Ibberson, M., Franklin, I., Binnert, C., Pende, M., Gjinovci, A., Hansotia, T., Drucker, D. J., Wollheim, C., and Burcelin, R. (2004) Gluco-incretins control insulin secretion at multiple levels as revealed in mice lacking GLP-1 and GIP receptors. *The Journal of clinical investigation* **113**, 635-645

52. Reimann, F., Habib, A. M., Tolhurst, G., Parker, H. E., Rogers, G. J., and Gribble, F. M. (2008) Glucose sensing in L cells: a primary cell study. *Cell metabolism* **8**, 532-539

53. Reimann, F., Maziarz, M., Flock, G., Habib, A., Drucker, D., and Gribble, F. (2005) Characterization and functional role of voltage gated cation conductances in the glucagon□like peptide□1 secreting GLUTag cell line. *The Journal of physiology* **563**, 161-175

54. Santos-Hernández, M., Reimann, F., and Gribble, F. M. (2024) Cellular mechanisms of incretin hormone secretion. *Journal of molecular endocrinology* **72**

55. Seino, Y., Maekawa, R., Ogata, H., and Hayashi, Y. (2016) Carbohydrate□induced secretion of glucose□dependent insulinotropic polypeptide and glucagon□like peptide□1. *Journal of diabetes investigation* **7**, 27-32

56. Seino, Y., Ogata, H., Maekawa, R., Izumoto, T., Iida, A., Harada, N., Miki, T., Seino, S., Inagaki, N., and Tsunekawa, S. (2015) Fructose induces glucose□dependent insulinotropic polypeptide, glucagon□like peptide□1 and insulin secretion: role of adenosine triphosphate□sensitive K+ channels. *Journal of Diabetes Investigation* **6**, 522-526

57. Stanhope, K. L., Schwarz, J. M., Keim, N. L., Griffen, S. C., Bremer, A. A., Graham, J. L., Hatcher, B., Cox, C. L., Dyachenko, A., and Zhang, W. (2009) Consuming fructose-sweetened, not glucose-sweetened, beverages increases visceral adiposity and lipids and decreases insulin sensitivity in overweight/obese humans. *The Journal of clinical investigation* **119**, 1322-1334

58. Sugimoto, K., Hosotani, T., Kawasaki, T., Nakagawa, K., Hayashi, S., Nakano, Y., Inui, H., and Yamanouchi, T. (2010) Eucalyptus leaf extract suppresses the postprandial elevation of portal, cardiac and peripheral fructose concentrations after sucrose ingestion in rats. *Journal of clinical biochemistry and nutrition* **46**, 205-211

59. Sun, E. W., De Fontgalland, D., Rabbitt, P., Hollington, P., Sposato, L., Due, S. L., Wattchow, D. A., Rayner, C. K., Deane, A. M., and Young, R. L. (2017) Mechanisms

controlling glucose-induced GLP-1 secretion in human small intestine. *Diabetes* **66**, 2144-2149

60. Tantama, M., Martínez-François, J. R., Mongeon, R., and Yellen, G. (2013) Imaging energy status in live cells with a fluorescent biosensor of the intracellular ATP-to-ADP ratio. *Nature communications* **4**, 2550

61. Taylor, S. R., Ramsamooj, S., Liang, R. J., Katti, A., Pozovskiy, R., Vasan, N., Hwang, S.-K., Nahiyaan, N., Francoeur, N. J., and Schatoff, E. M. (2021) Dietary fructose improves intestinal cell survival and nutrient absorption. *Nature* **597**, 263-267

62. Ter Horst, K. W., Schene, M. R., Holman, R., Romijn, J. A., and Serlie, M. J. (2016) Effect of fructose consumption on insulin sensitivity in nondiabetic subjects: a systematic review and meta-analysis of diet-intervention trials. *The American journal of clinical nutrition* **104**, 1562-1576

63. Yabe D, Kuroe A, Watanabe K, Iwasaki M, Hamasaki A, Hamamoto Y, Harada N, Yamane S, Lee S, Murotani K, Deacon CF, Holst JJ, Hirano T, Inagaki N, Kurose T, and Seino Y. (2015) Early phase glucagon and insulin secretory abnormalities, but not incretin secretion, are similarly responsible for hyperglycemia after ingestion of nutrients. *J Diabetes Complications* **29**, 413-421.

64. Zawalich, W. S., Rognstad, R., Pagliara, A. S., and Matschinsky, F. M. (1977) A comparison of the utilization rates and hormone-releasing actions of glucose, mannose, and fructose in isolated pancreatic islets. *J Biol Chem* **252**, 8519-8523

FIGURE CAPTIONS

Graphical Abstract

This study investigated the hormonal effects of short-term fructose consumption in mice, allowing them ad-lib access to fructose solution for 24 h. Fructose metabolism in intestinal L-cells increases the intracellular ATP/ADP ratio, leading to GLP-1 secretion via K_{ATP} channel closure and Ca^{2+} influx. GLP-1 promotes insulin secretion from pancreatic β-cells. The fructose metabolism/GLP-1/insulin pathway is essential for mitigation of fructose-induced hyperglycemia.

Parts of the figure were drawn using pictures from Servier Medical Art by Servier licensed under a CC-BY 4.0 with color modification.

Figure 1. Short-term fructose ingestion in lean and diabetic mice

A. Schematic illustration of short-term fructose administration. Parts of the figure were drawn using pictures from Servier Medical Art by Servier licensed under a Creative Commons Attribution 4.0 International License (CC-BY 4.0) with color modification.

B. Blood glucose levels following 24-hour fructose ingestion. *a*/*a* Fru -: n = 18; *a*/*a* Fru +: n = 20; A^y/*a* Fru -: n = 18; A^y/*a* Fru +: n = 17. N = 3.

C. Plasma insulin levels following 24-hour fructose ingestion. *a*/*a* Fru -: n = 18; *a*/*a* Fru +: n = 20; A^y/*a* Fru -: n = 14; A^y/*a* Fru +: n = 14. N = 2.

D. –G. Oral glucose tolerance test (OGTT) following 24-hour fructose ingestion. D, Blood glucose levels. E, Area under the curve (AUC) of blood glucose levels. *a*/*a* Fru -: n = 6; *a*/*a* Fru +: n = 6; A^y/*a* Fru -: n = 6; A^y/*a* Fru +: n = 6. N = 2. F, Plasma insulin levels. E, Area under the curve (AUC) of plasma insulin levels. *a*/*a* Fru -: n = 8; *a*/*a* Fru +: n = 9; A^y/*a* Fru -: n = 5; A^y/*a* Fru +: n = 5. N = 2.

Data are presented as the mean ± standard deviation (SD). Fru -: water-administered mice, Fru +: fructose-administered mice. Statistical comparisons were performed using Welch's two-way ANOVA with Dunnett's post-hoc test.

Figure 2. Involvement of plasma fructose, GLP-1, and GIP in the fructose-induced plasma insulin response.

A. –D. Plasma concentrations of fructose, total GLP-1, and total GIP following 24-hour fructose ingestion. A. Fructose levels in the tail vein. *a*/*a* Fru -: n = 6; *a*/*a* Fru +: n = 6; A^y/*a* Fru -: n = 6; A^y/*a* Fru +: n = 6. N = 2. B, Fructose levels in the portal vein. *a*/*a* Fru -: n = 5; *a*/*a* Fru +: n = 6; A^y/*a* Fru -: n = 6; A^y/*a* Fru +: n = 6. N = 2. C, total GLP-1. *a*/*a* Fru -: n = 12; *a*/*a* Fru +: n = 15; *Ay*/*a* Fru -: n = 10; A^y/*a* Fru +: n = 9. N = 2. D, total GLP-1. *a*/*a* Fru -: n = 13; *a*/*a* Fru +: n = 15; A^y/*a* Fru -: n = 10; A^y/*a* Fru +: n = 10. N = 2.

E. Effect of exendin [9-39] on fructose-induced insulin response. Exendin [9-39] (100 nmol/kg) was intraperitoneally injected following 24-hour fructose ingestion. Time-dependent changes in plasma insulin levels before and after injection are shown. n = 9, N = 2.

F. –G. Insulin secretory responses to GLP-1 and GIP in isolated islets. F, *a*/*a* mouse islets. n = 5. Islets were pooled from two mice. G, A^y/*a* mouse islets. n = 6. Islets were pooled from two mice. N = 2.

Data are presented as the mean ± standard deviation (SD). Fru -: water-administered mice, Fru +: fructose-administered mice. Statistical comparisons were performed using Welch's one-way ANOVA with Dunnett's post-hoc test except for E. Welch's unpaired two-tailed t-test was used for E.

Figure 3. Involvement of GLP-1 and GIP in fructose-induced metabolic responses.

(A, E, H) Blood glucose, (B, F, I) insulin, (C, J) total GLP-1, and (D, G, K) total GIP levels were measured following 24-hour fructose ingestion in multiple strains of mice.

A. –D: B6 mice. A: n = 12; B: n = 9; C: n = 6; D: n = 12. N = 2.

E. –G: *Gcg*$^{-/-}$ mice. E: n = 9; F: n = 9; G: n = 12. N = 2.

H. –K: *Gipr*$^{-/-}$ mice. H, Fru -: n = 10; Fru +: n = 9; I, Fru -: n = 16; Fru +: n = 14; J, Fru -: n = 4; Fru +: n = 5; K, Fru -: n = 10; Fru +: n = 10. N = 2.

Data are presented as the mean ± standard deviation (SD). Statistical comparisons were made using Welch's unpaired two-tailed t-test.

Figure 4. Metabolism-secretion coupling in fructose-induced GLP-1 secretion in GLUTag cells.

A. Dose-dependent effect of fructose on GLP-1 secretion. n = 6. N = 3.

B. –C. Effect of fructose on the intracellular ATP/ADP ratio as visualized by Perceval-HR. Effects of *Khk* and *Aldob* knockdown were tested and time course of normalized ratiometric signals (R/R0) are indicated in B (NT: n = 26; *Khk*: n = 38) and C (NT: n = 26; *Aldob*: n = 27), respectively. N = 2. For statistical analyses, see Supplementary Figure 3, C–D.

D. Effect of fructose on intracellular Ca^{2+} visualized by Fluo-4. Effects of *Khk* and *Aldob* knockdown are tested. Representative traces of normalized fluorescence (F/F0) are shown. For statistical analyses, see Supplementary Figure 3, E–F. N = 2.

E. Effects of *Khk* and *Aldob* knockdown on fructose-induced GLP-1 secretion. n = 4. N = 2.

F. Effect of TEPP-46 (10 μM) on fructose-induced increase in intracellular ATP/ADP ratio, as visualized by Perceval-HR. TEPP-46 -: n = 32; TEPP-46 +: n = 45. The time course of the normalized ratiometric signals (R/R0) is shown. For statistical analyses, see Supplementary Figure 3G. N = 2.

G. Effects of TEPP-46 (10 μM) and nifedipine (10 μM) on fructose-induced GLP-1 secretion. n = 6. N = 2.

H. Effect of nifedipine (10 μM) on fructose-induced Ca^{2+} response as visualized by Fluo-4. Representative traces of normalized fluorescence (F/F0) are shown. For statistical analysis, see Supplementary Figure 3, H–I. N = 2.

I. (B) The magnitude of the responses was quantified as iAUC using R/R0 = 1 as the baseline.

J. –(D) [U-^{13}C]-fructose tracing under *Khk* knockdown in MIN6-K8 cells. The total content and isotopic distribution of F1P are presented in (C). The fraction of ^{13}C in each intermediate is presented in (D). n = 4. See Supplementary Figure 2 for the total content of other metabolites.

K. The effect of *Khk* knockdown on FSIS was expressed as fold change over 0 mM fructose. See Supplementary Figure 3D for the original values.

All experiments were performed using GLUTag cells. For the imaging experiments, 10 mM fructose was loaded from t = 0. siNT, non-targeting siRNA. Data are presented as the mean ± SD. Statistical comparisons were performed using Welch's one-way ANOVA with Dunnett's post-hoc test for A, and two-way ANOVA with Šídák's multiple comparisons post-hoc test for E and G.

Figure 5. Involvement of K_{ATP} channels in fructose-induced GLP-1 and GIP secretion in vivo.

A. –D. (A) Blood glucose, (B) insulin, (C) total GLP-1, and (D) total GIP levels in *Kcnj11*$^{-/-}$ mice following 24-hour fructose ingestion. A–C, Fru -: n = 6; Fru -: n = 5. D, Fru -: n = 12; Fru -: n = 11.

E. –F. Effect of diazoxide (Dz) on fructose-induced GLP-1 and GIP responses in *a*/*a* mice. Diazoxide (10 mM) was added to the water or fructose solution. Incretin levels were measured following 24-hour fructose ingestion. (E) Total GLP-1, Fru - Dz -: n = 7; Fru + Dz -: n = 8; Fru - Dz +: n = 6; Fru + Dz +: n = 7. (F) Total GIP, Fru - Dz -: n = 7; Fru + Dz -: n = 6; Fru - Dz +: n = 10; Fru + Dz +: n = 12.

Data are presented as the mean ± SD. Statistical comparisons were performed using Welch's unpaired two-tailed t-test for A–D, and Welch's one-way ANOVA with Dunnett's post-hoc test for E–F.

Figure 6. Fructose metabolic tracing in isolated intestinal crypts of lean and diabetic mice.

A. Schematic overview of the potential metabolic fate of $^{13}C_6$-fructose. G6P, glucose 6-phosphate; F6P, fructose 6-phosphate; F1P, fructose 1-phosphate; GA3P, glyceraldehyde 3-phosphate; DHAP, dihydroxyacetone phosphate; G3P, glycerol 3-phosphate; OXPHOS, oxidative phosphorylation. M2–M6 denote isotopomers with 0-6 carbon atoms substituted by ^{13}C.

B. –I. $^{13}C_6$-fructose tracing in intestinal crypts isolated from *a*/*a* and A^y/a mice. Only Isotopomers converted from $^{13}C_6$-fructose are indicated. See Supplementary Figure 4 for comprehensive results, including the other isotopomers. n = 6 for each condition. N = 2.

J. –L. Adenosine nucleotide content in $^{13}C_6$-fructose tracing. Only unlabelled isotopomers [M0] were analyzed. n = 6 for each condition. N = 2.

Data are presented as the mean ± SD. ND, not detected. Statistical comparisons were performed using Welch's unpaired two-tailed t-test for B–I and two-way ANOVA with Uncorrected Fisher's Fisher's Least Significant Difference test for J–L. For H and I, the sum of all the indicated isotopomers was compared.

Supplementary Figure 1.

A. –B. Age-dependent changes in (A) body weight and (B) ad-lib fed blood glucose in NSY.B6 strains. n = 6 for each strain. N = 2.

C. –D. Intraperitoneal insulin tolerance test (IPITT) following 24-hour fructose ingestion. C, Blood glucose levels are expressed as % at 0 min. D, AUC of blood glucose levels. *a*/*a* Fru -: n = 5; *a*/*a* Fru +: n = 5; A^y/a Fru -: n = 4; A^y/a Fru +: n = 4. N = 2.

Age-dependent changes in ad-lib fed blood glucose levels in NSY.B6 strains. Statistical comparisons were made using Welch's unpaired two-tailed t-test at each age in A and B, and Welch's one-way ANOVA with Dunnett's post-hoc test for D.

Supplementary Figure 2.

A. –B. Plasma fructose levels following oral administration of fructose (2 g/kg). (A) NSY.B6 mouse strains. n = 5 for each strain. (B) B6 mice. n = 5. N = 2.

C. Plasma glucagon levels following 24-hour fructose ingestion in *a*/*a* mice. n = 5. N = 2.

Data are presented as the mean ± SD. Statistical comparisons were made using Welch's unpaired two-tailed t-test.

Supplementary Figure 3.

A. –B. Knockdown efficiency of (A) *Khk* and (B) *Aldob* was assessed by RT-qPCR. mRNA levels were normalized to those in siNT (non-targeting siRNA)-treated cells. n = 4, N = 2.

C. –D. Effect of *Khk* and *Aldob* knockdown on fructose-stimulated ATP/ADP ratio in GLUTag cells. iAUC of Perceval-HR ratiometric signals (R/R0) are indicated in B (NT: n = 26; *Khk*: n = 38) and C (NT: n = 26; *Aldob*: n = 27), respectively. N = 2. The original values are shown in Figures 4B and 4C.

E. –F. Effect of *Khk* and *Aldob* knockdown on fructose-stimulated $[Ca^{2+}]i$ changes visualized using Fluo-4. E, Time course of the averages of normalized fluorescence intensity (F/F0) is indicated. For representative traces, see Figure 4D. F, the magnitude of $[Ca^{2+}]i$ responses was quantified as iAUC using F/F0 =1 as the baseline. siNT: n = 41; 8.8 mM si*Khk*: n = 40; si*Aldob*: n = 46. N = 2.

G. Effect of TEPP-46 on the ATP/ADP ratio in GLUTag cells. iAUC of Perceval-HR ratiometric signals (R/R0) are indicated. For the original values, see Figure 4F. TEPP-46 -: n = 32; TEPP-46 +: n = 45. N = 2.

H. –I. Effect of nifedipine (Nife) on fructose-stimulated intracellular Ca^{2+} changes visualized using Fluo-4. H, Time course of the averages of normalized fluorescence intensity (F/F0) is indicated. For representative traces, see Figure 4D. I: The magnitude of $[Ca^{2+}]i$ responses was quantified as iAUC using F/F0 =1 as the baseline. DMSO: n = 18; Nife: n = 20. N = 2.

Data are presented as the mean ± SD. Statistical comparisons were made using Welch's one-way ANOVA with Dunnett's post-hoc test for F, and Welch's unpaired two-tailed t-test for the other results.

Supplementary Figure 4.

A. Fluorescence microscopy images of freshly isolated intestinal crypts from *Gcg*$^{gfp/+}$ mice.

B. –I. $^{13}C_6$-fructose tracing in MIN6-K8 cells. n = 4. The total content and isotopic distribution of each intermediate are presented as stacked bar graphs. n = 4. N = 2

Statistical comparisons were made between the sum of all indicated isotopomers using Welch's unpaired two-tailed t-test.

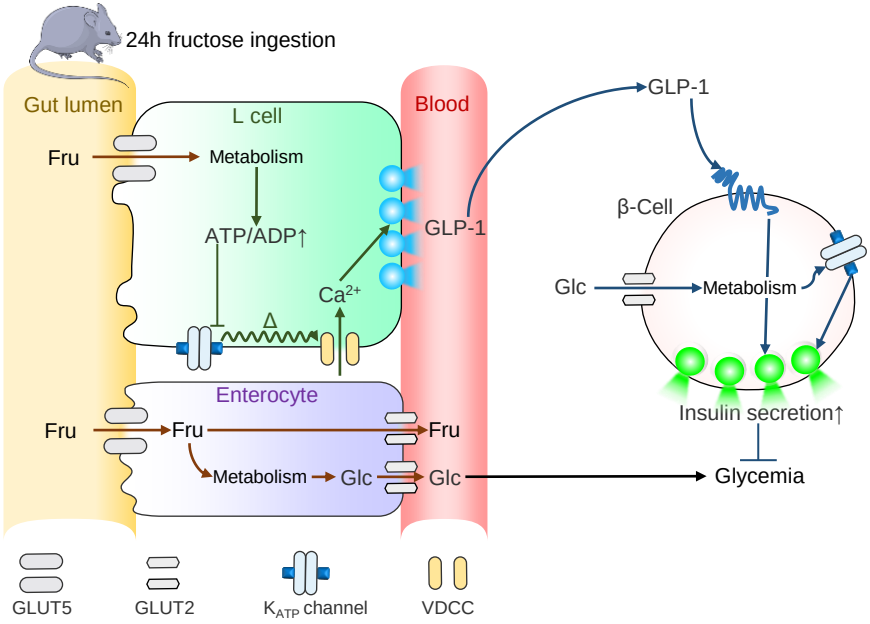

Graphical abstract

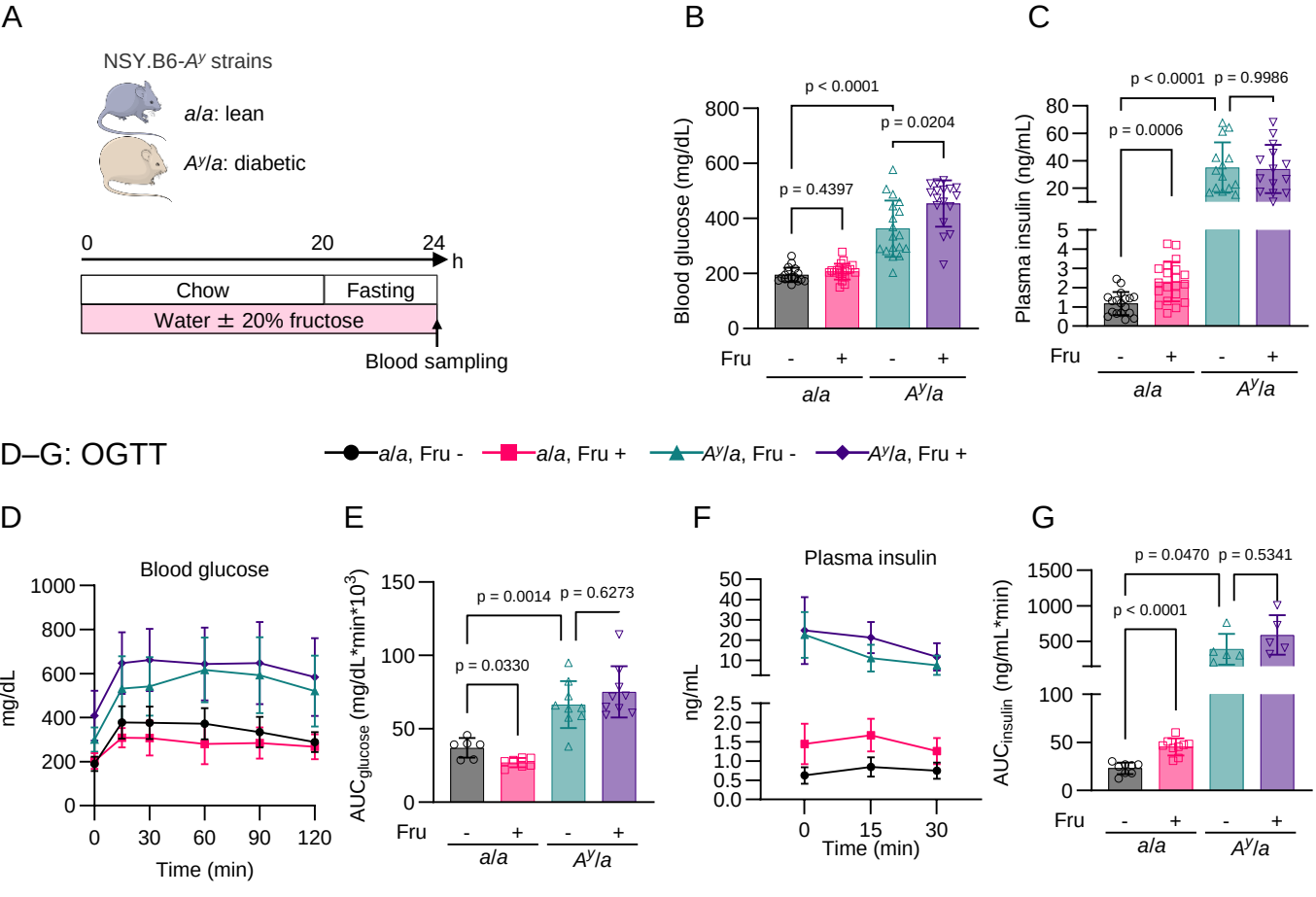
A
NSY.B6-Aʸ strains
a/a: lean
Aʸ/a: diabetic
0
20
24
h
Chow
Fasting
Water ± 20% fructose
Blood sampling
B
Blood glucose (mg/dL)
p < 0.0001
p = 0.0204
p = 0.4397
Fru
a/a
Aʸ/a
C
Plasma insulin (ng/mL)
p < 0.0001
p = 0.9986
p = 0.0006
D–G: OGTT
a/a, Fru -
a/a, Fru +
Aʸ/a, Fru -
Aʸ/a, Fru +
D
Blood glucose
mg/dL
Time (min)
E
AUCglucose (mg/dL*min*10³)
p = 0.0014
p = 0.6273
p = 0.0330
F
Plasma insulin
ng/mL
Time (min)
G
AUCinsulin (ng/mL*min)
p = 0.0470
p = 0.5341
p < 0.0001

Figure 1.

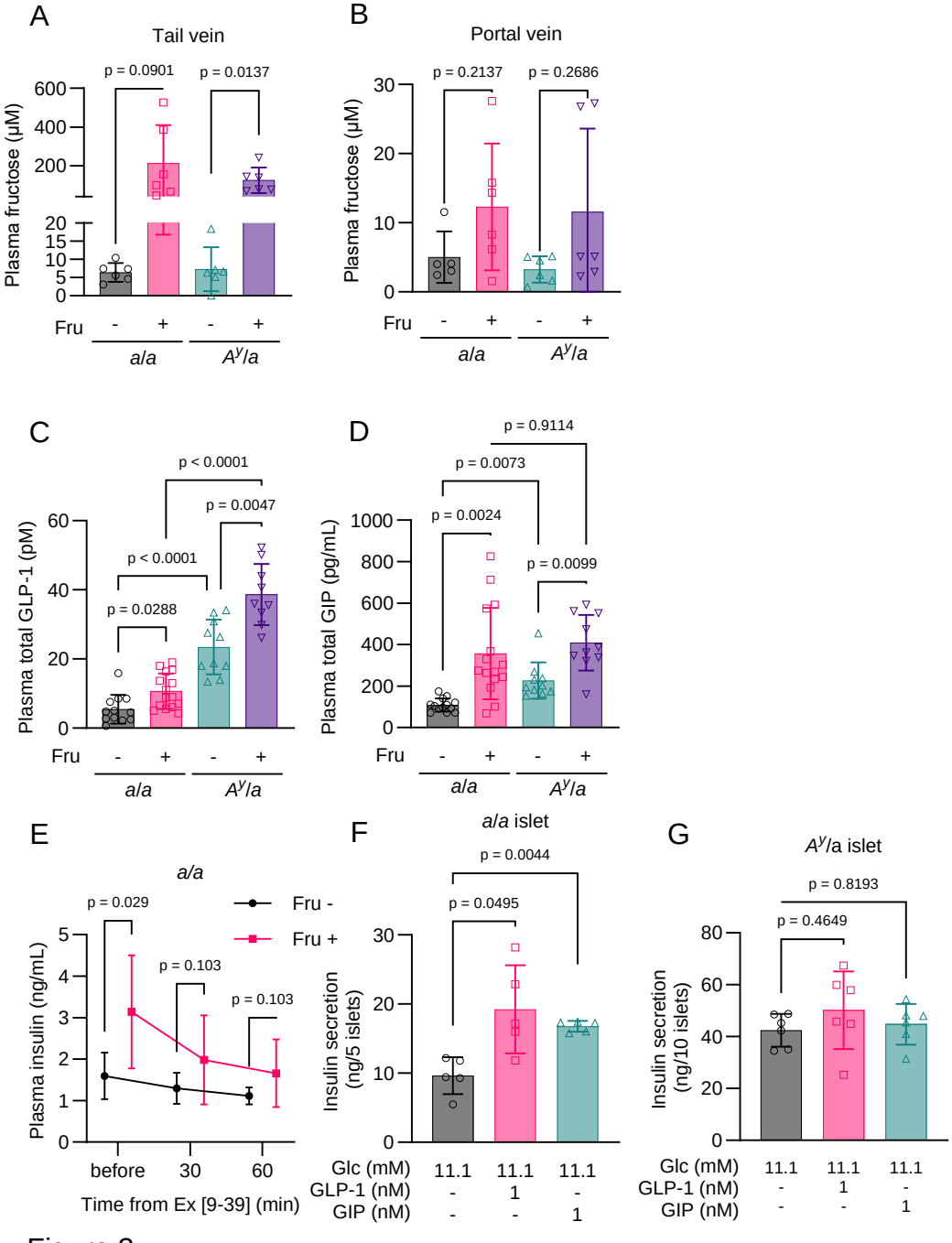
A
Tail vein
p = 0.0901
p = 0.0137
Plasma fructose (μM)
600
400
200
20
15
10
5
0
Fru - + - +
a/a
A^y/a
B
Portal vein
p = 0.2137
p = 0.2686
Plasma fructose (μM)
30
20
10
0
Fru - + - +
a/a
A^y/a
C
p < 0.0001
p = 0.0047
p < 0.0001
p = 0.0288
Plasma total GLP-1 (pM)
60
40
20
0
Fru - + - +
a/a
A^y/a
D
p = 0.9114
p = 0.0073
p = 0.0024
p = 0.0099
Plasma total GIP (pg/mL)
1000
800
600
400
200
0
Fru - + - +
a/a
A^y/a
E
a/a
p = 0.029
p = 0.103
p = 0.103
Fru -
Fru +
Plasma insulin (ng/mL)
5
4
3
2
1
0
before
30
60
Time from Ex [9-39] (min)
F
a/a islet
p = 0.0044
p = 0.0495
Insulin secretion (ng/5 islets)
30
20
10
0
Glc (mM) 11.1 11.1 11.1
GLP-1 (nM) - 1 -
GIP (nM) - - 1
G
A^y/a islet
p = 0.8193
p = 0.4649
Insulin secretion (ng/10 islets)
80
60
40
20
0
Glc (mM) 11.1 11.1 11.1
GLP-1 (nM) - 1 -
GIP (nM) - - 1

Figure 2.

A–D: B6

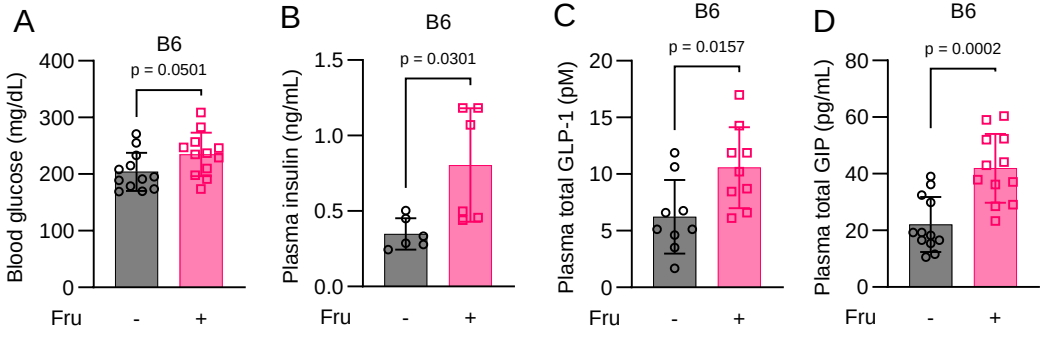

E–G: *Gcg*$^{-/-}$

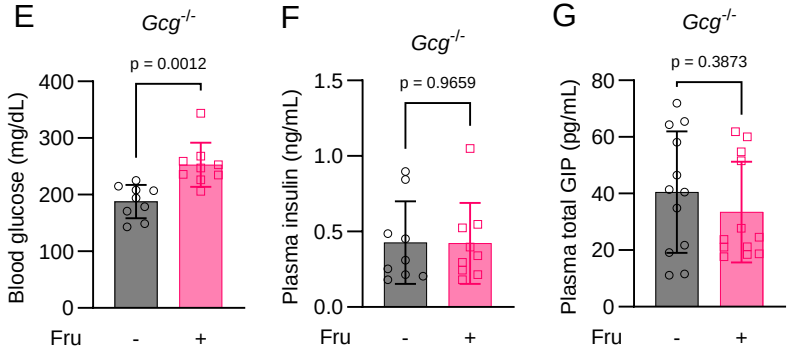

H–K: *Gipr*$^{-/-}$

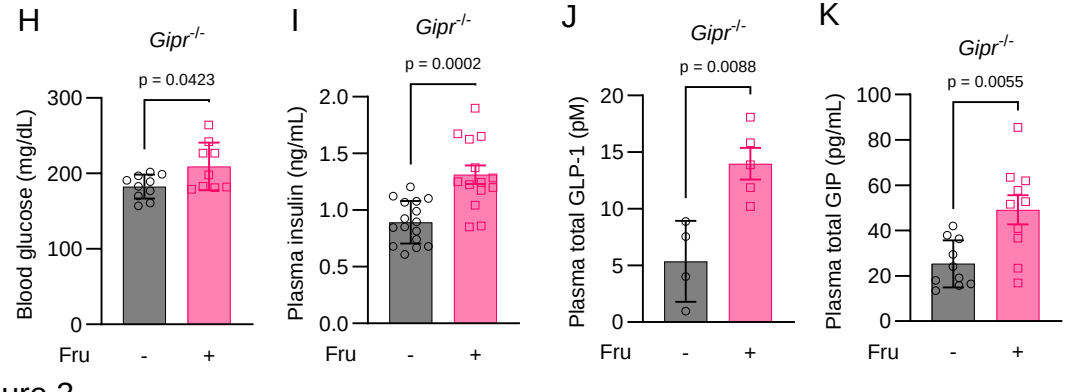

Figure 3.

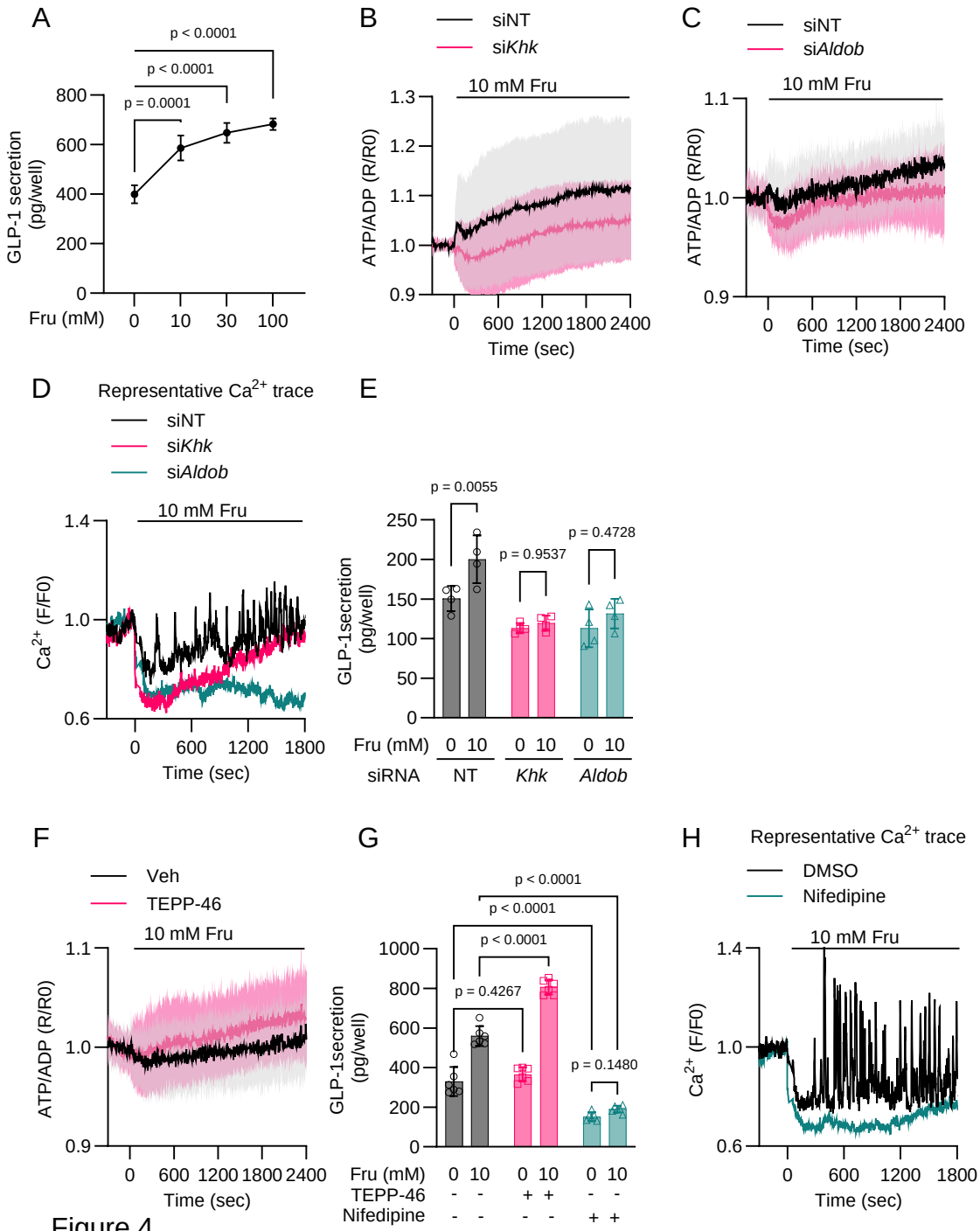
A
p < 0.0001
p < 0.0001
p = 0.0001
GLP-1 secretion (pg/well)
800
600
400
200
0
Fru (mM)
0
10
30
100
B
siNT
siKhk
10 mM Fru
ATP/ADP (R/R0)
1.3
1.2
1.1
1.0
0.9
0
600
1200
1800
2400
Time (sec)
C
siNT
siAldob
10 mM Fru
ATP/ADP (R/R0)
1.1
1.0
0.9
0
600
1200
1800
2400
Time (sec)
D
Representative Ca2+ trace
siNT
siKhk
siAldob
10 mM Fru
Ca2+ (F/F0)
1.4
1.0
0.6
0
600
1200
1800
Time (sec)
E
p = 0.0055
p = 0.9537
p = 0.4728
GLP-1secretion (pg/well)
250
200
150
100
50
0
Fru (mM)
0
10
0
10
0
10
siRNA
NT
Khk
Aldob
F
Veh
TEPP-46
10 mM Fru
ATP/ADP (R/R0)
1.1
1.0
0.9
0
600
1200
1800
2400
Time (sec)
G
p < 0.0001
p < 0.0001
p < 0.0001
p = 0.4267
p = 0.1480
GLP-1secretion (pg/well)
1000
800
600
400
200
0
Fru (mM)
0
10
0
10
0
10
TEPP-46
-
-
+
+
-
-
Nifedipine
-
-
-
-
+
+
H
Representative Ca2+ trace
DMSO
Nifedipine
10 mM Fru
Ca2+ (F/F0)
1.4
1.0
0.6
0
600
1200
1800
Time (sec)

Figure 4.

A–D: *Kcnj11*$^{-/-}$

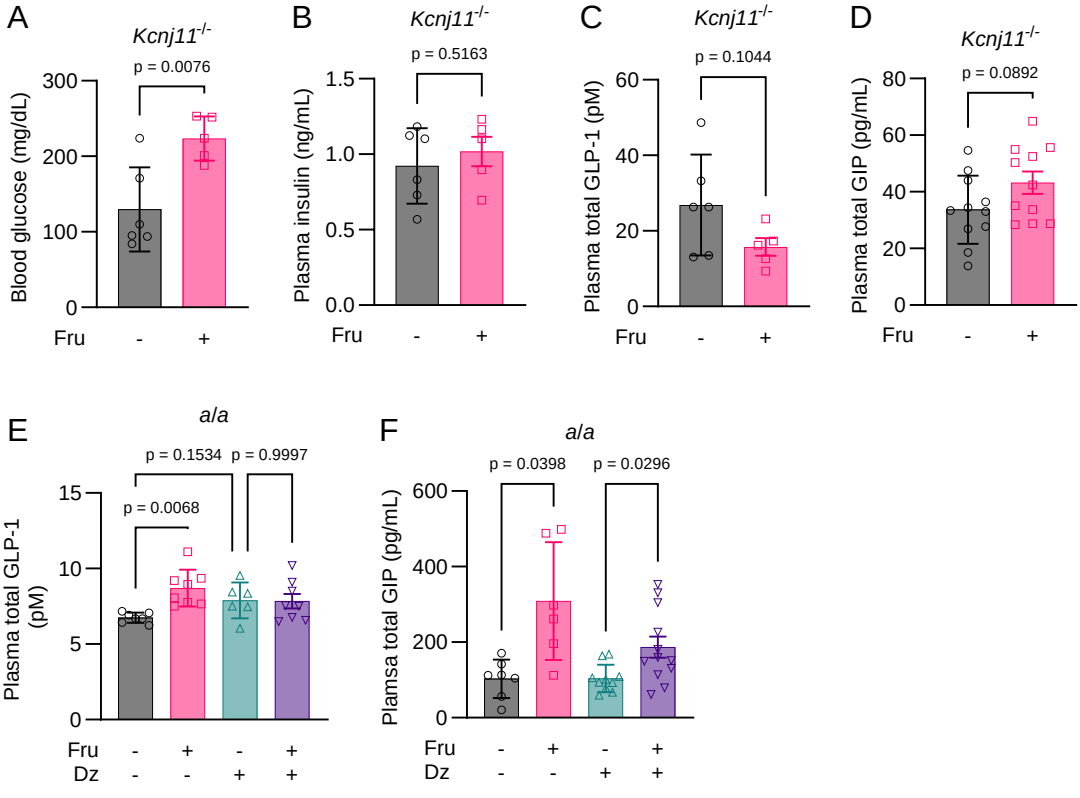

Figure 5.

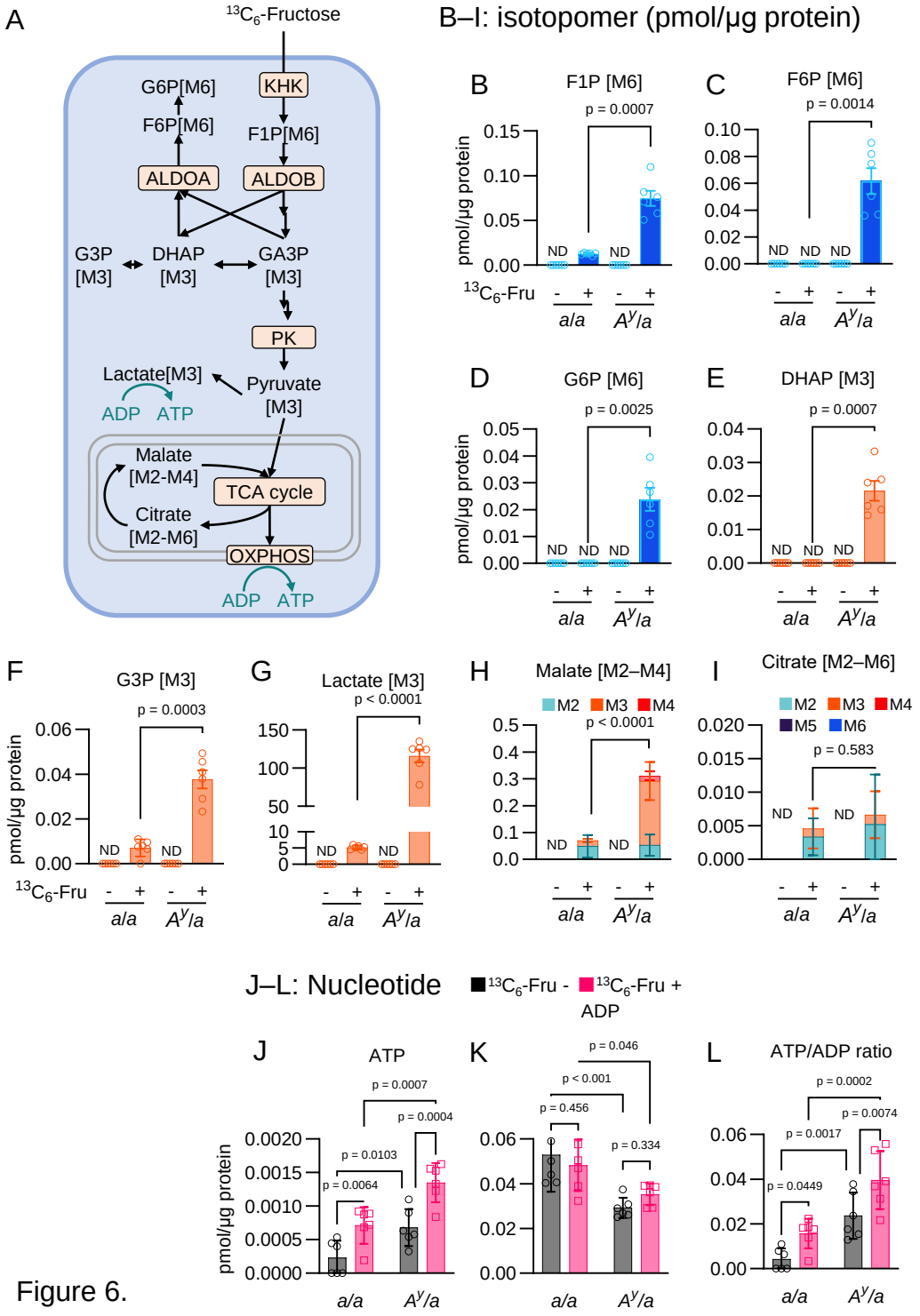
A
13C6-Fructose
KHK
G6P[M6]
F6P[M6]
F1P[M6]
ALDOA
ALDOB
G3P [M3]
DHAP [M3]
GA3P [M3]
PK
Lactate[M3]
Pyruvate [M3]
ADP ATP
Malate [M2-M4]
TCA cycle
Citrate [M2-M6]
OXPHOS
ADP ATP
B–I: isotopomer (pmol/µg protein)
B F1P [M6]
p = 0.0007
C F6P [M6]
p = 0.0014
D G6P [M6]
p = 0.0025
E DHAP [M3]
p = 0.0007
F G3P [M3]
p = 0.0003
G Lactate [M3]
p < 0.0001
H Malate [M2–M4]
M2 M3 M4
p < 0.0001
I Citrate [M2–M6]
M2 M3 M4 M5 M6
p = 0.583
pmol/µg protein
ND
13C6-Fru - + - +
a/a Ay/a
J–L: Nucleotide
13C6-Fru - 13C6-Fru + ADP
J ATP
p = 0.0007
p = 0.0004
p = 0.0103
p = 0.0064
K
p = 0.046
p < 0.001
p = 0.456
p = 0.334
L ATP/ADP ratio
p = 0.0002
p = 0.0074
p = 0.0017
p = 0.0449

Figure 6.

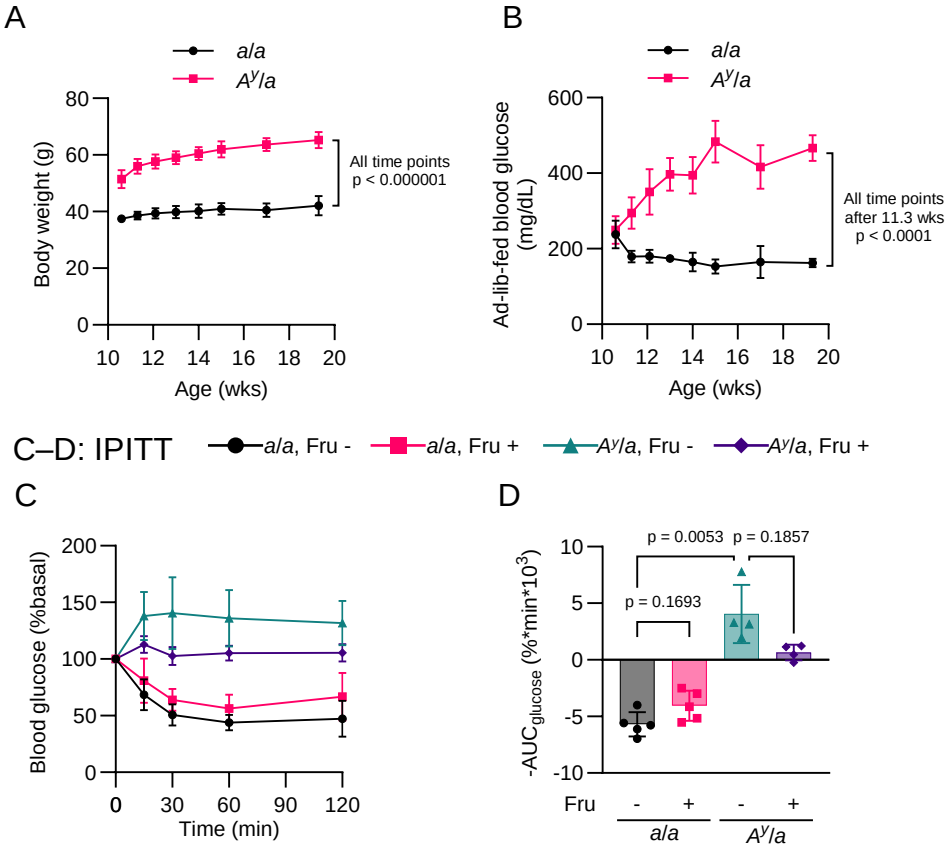

Supplementary Figure 1.

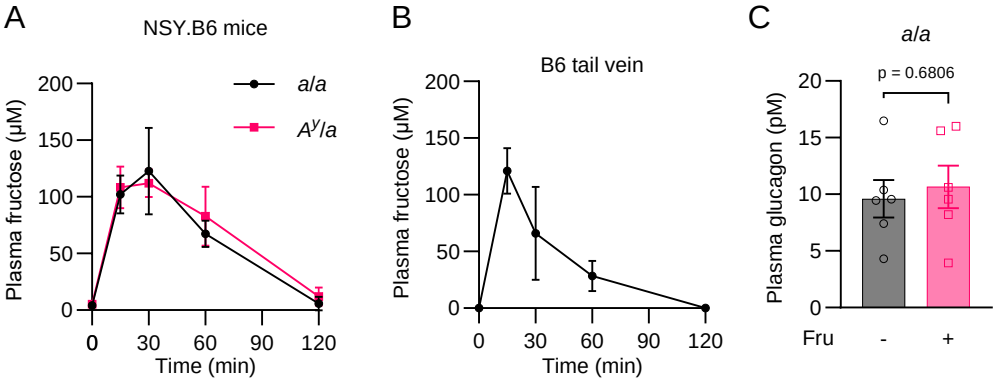

Supplementary Figure 2.

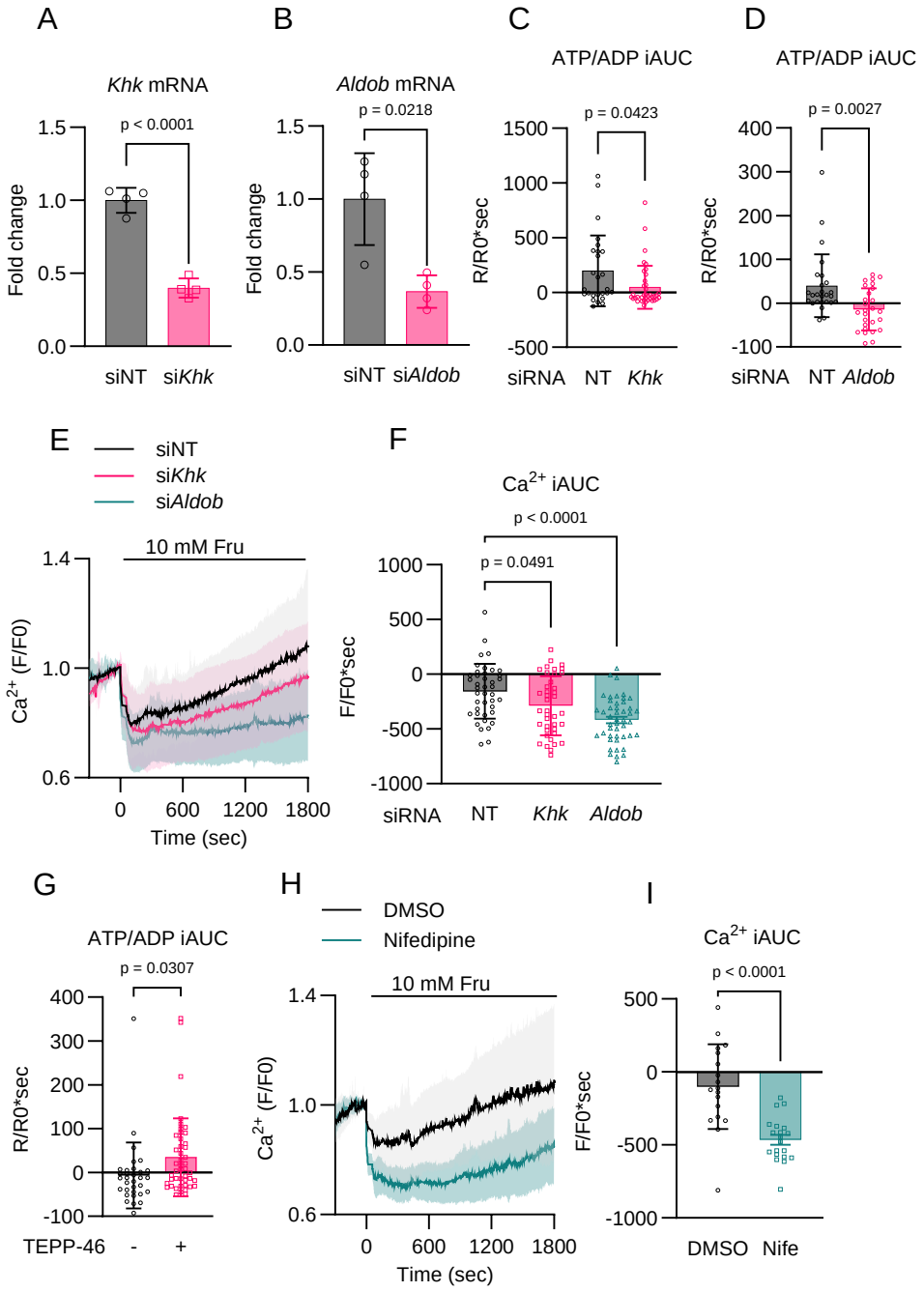

Supplementary Figure 3.

A: isolated intestinal crypts (*Gcg*$^{gfp/+}$)

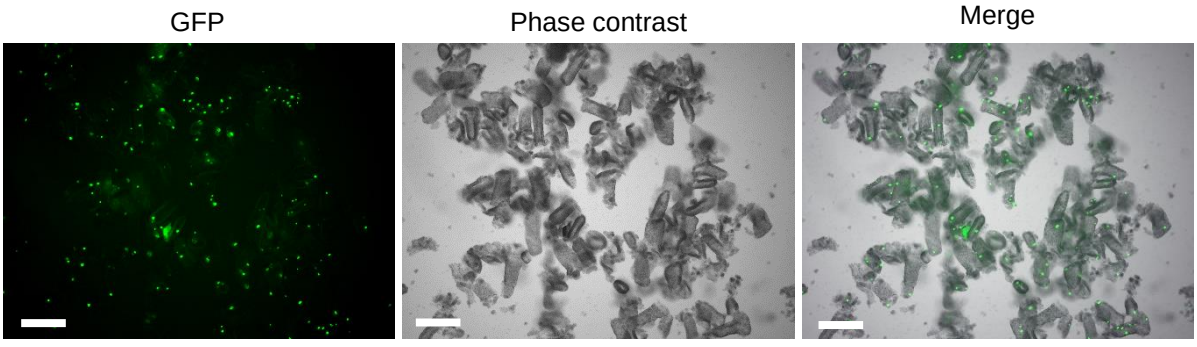

Scale bars, 1mm.

B–I: isotopomers

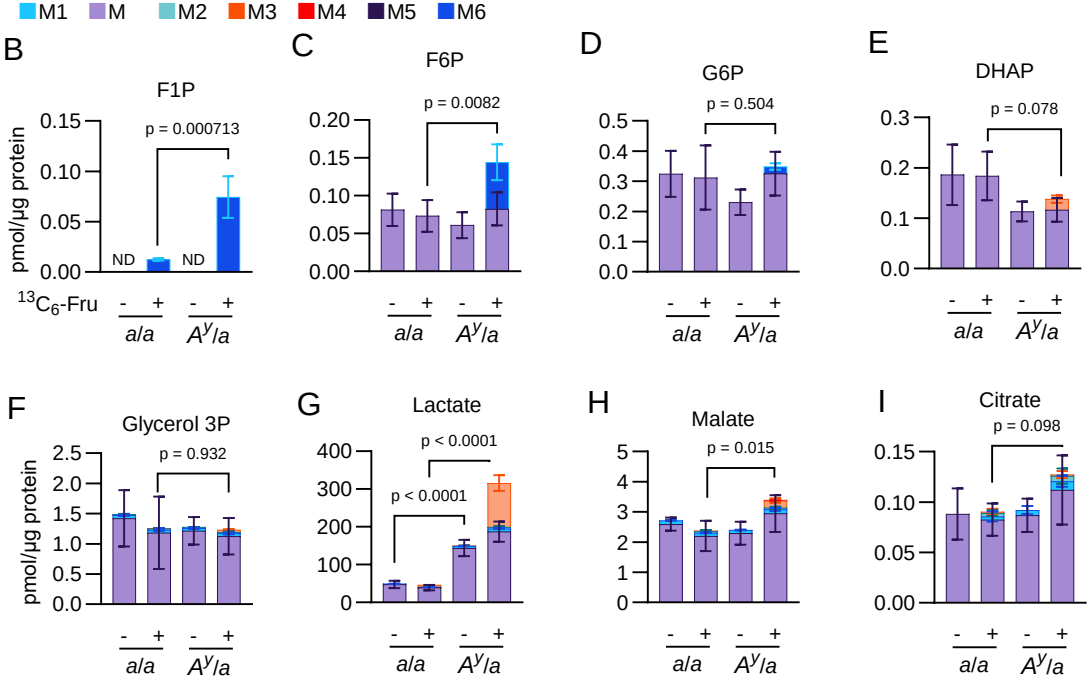

Supplementary Figure 4.